frontiers in Ecology and Evolution

ORIGINAL RESEARCH
published: 10 March 2022
doi: 10.3389/fevo.2021.799637

Modeling Skull Network Integrity at the Dawn of Amniote Diversification With Considerations on Functional Morphology and Fossil Jaw Muscle Reconstructions

Ingmar Werneburg[1,2]* *and Pascal Abel*[1,2]

[1] Senckenberg Centre for Human Evolution and Palaeoenvironment at Eberhard Karls Universität Tübingen, Tübingen, Germany, [2] Fachbereich Geowissenschaften der Eberhard Karls Universität Tübingen, Tübingen, Germany

One of the major questions in evolutionary vertebrate morphology is the origin and meaning of temporal skull openings in land vertebrates. Partly or fully surrounded by bones, one, two, or even three openings may evolve behind the orbit, within the ancestrally fully roofed anapsid (*scutal*) skull. At least ten different morphotypes can be distinguished in tetrapods with many modifications and transitions in more crownward representatives. A number of potential factors driving the emergence and differentiation of temporal openings have been proposed in the literature, but only today are proper analytical tools available to conduct traceable tests for the functional morphology underlying temporal skull constructions. In the present study, we examined the anatomical network in the skull of one representative of early amniotes, †*Captorhinus aguti*, which ancestrally exhibits an anapsid skull. The resulting skull modularity revealed a complex partitioning of the temporal region indicating, in its intersections, the candidate positions for potential infratemporal openings. The framework of †*C. aguti* was then taken as a template to model a series of potential temporal skull morphotypes in order to understand how skull openings might influence the modular composition of the amniote skull in general. We show that the original pattern of skull modularity (†*C. aguti*) experiences comprehensive changes by introducing one or two temporal openings in different combinations and in different places. The resulting modules in each skull model are interpreted in regard to the feeding behavior of amniotes that exhibit(ed) the respective skull morphotypes. An important finding is the alternative incorporation of the jugal and palate to different modules enforcing the importance of an integrated view on skull evolution: the temporal region cannot be understood without considering palatal anatomy. Finally, we discuss how to better reconstruct relative jaw muscle compositions in fossils by considering the modularity of the skull network. These considerations might be relevant for future biomechanical studies on skull evolution.

Keywords: Amniota, Reptilia, biomechanics, cranial osteology, temporal skull openings, fenestration

OPEN ACCESS

Edited by:
Michel Laurin,
UMR 7207 Centre de Recherche sur la Paléobiodiversité et les Paléoenvironnements (CR2P), France

Reviewed by:
Diego Rasskin-Gutman,
University of Valencia, Spain
Eduardo Ascarrunz,
Université de Fribourg, Switzerland

***Correspondence:**
Ingmar Werneburg
ingmar.werneburg@senckenberg.de

Specialty section:
This article was submitted to Paleontology, a section of the journal Frontiers in Ecology and Evolution

Received: *21 October 2021*
Accepted: *22 December 2021*
Published: *10 March 2022*

Citation:
Werneburg I and Abel P (2022) Modeling Skull Network Integrity at the Dawn of Amniote Diversification With Considerations on Functional Morphology and Fossil Jaw Muscle Reconstructions. Front. Ecol. Evol. 9:799637. doi: 10.3389/fevo.2021.799637

INTRODUCTION

The evolutionary transition from a mostly aquatic to a fully terrestrial life in vertebrates is associated with a number of fundamental anatomical and physiological changes (Sumida and Martin, 1997; Laurin, 2010; Clack, 2012). These include the evolution of an encapsuled (i.e., amniotic) egg with extraembryonic membranes and the loss of a larval stage in development (Laurin, 2005). As a consequence, morphological adaptative constraints to larval aquatic feeding were skipped, permitting within a few million years an enormous radiation of new feeding types with associated anatomical structures in the early amniotes (Werneburg, 2019). Concurrently, a transition from a primarily suction feeding behavior (Heiss et al., 2013; Natchev et al., 2015) toward a herbivorous (Weishampel, 1997; Sues and Reisz, 1998) or hunting behavior with a weapon-like jaw apparatus (Hülsmann and Wahlert, 1972) took place.

Feeding musculature mainly attaches to the temporal skull region behind the eye and to the posterior part of the palate (Holliday and Witmer, 2007; Jones et al., 2009; Diogo and Abdala, 2010; Werneburg, 2011; Ziermann et al., 2019). In both skull regions, major changes emerged, easily recognizable in all amniote skulls (Lakjer, 1926, 1927; Hanken and Hall, 1993a,b; Novacek, 1993; Rieppel, 1993; Zusi, 1993). In particular, the temporal skull region received much attention in the scientific literature, historically resulting in taxonomic groups mainly defined by the anatomy of their temporal skull region (e.g., Synapsida, Diapsida, "Anapsida"; Case, 1898; Williston, 1904; Broom, 1922; Zdansky, 1923; Frazzetta, 1968; Kuhn-Schnyder, 1980; Rieppel and Gronowski, 1981; Smith et al., 1983; Rieppel, 1984; Frey et al., 2001; Tarsitano et al., 2001; Müller, 2003; Cisneros et al., 2004; Werneburg, 2012, 2013a, 2015, 2019; Haridy et al., 2016; Elzanowski and Mayr, 2018; Abel and Werneburg, 2021) with only few of them still used today. This is because with the rise of phylogenetic systematics and the inclusion of hundreds of other anatomical characters, along with new fossil finds, a more comprehensive picture on amniote interrelationships has been developed (Abel and Werneburg, 2021). Nowadays, the temporal openings are only conditionally relevant for phylogenetic reconstructions. However, they can still be informative on selected phylogenetic levels and in particular taxonomic groups (Ford, 2018) and are considered as highly relevant to understand morphofunctional relationships within the skull.

Recently, Abel and Werneburg (2021) provided a comprehensive review on the diversity and the scientific history of the temporal skull region in land vertebrates. They defined ten skull morphotypes and discussed a series of potential functional factors that shape their temporal region. Proper tests to validate and quantify biomechanical parameters in temporal skull diversification, however, are still lacking.

In the present contribution, we used Anatomical Network Analysis (AnNA; Rasskin-Gutman and Esteve-Altava, 2014) to provide new insights into the complex construction of land vertebrate skulls (Werneburg et al., 2019). For this, we focused on the early Permian †*Captorhinus aguti* (Amniota, Captorhinidae), an early amniote that is known from a high number of three-dimensionally preserved skulls. Even though all major skull morphotypes evolved pretty early after the amniote origin, the skull of captorhinids remained ancestrally anapsid (*scutal sensu* Abel and Werneburg, 2021) with no temporal openings. After analyzing the skull of †*C. aguti*, we used it as a template by removing selected connections to create different skull models in order to estimate which influence the presence of particular temporal openings has on skull integrity. This, in turn, allowed first attempts to interpret alternative functionally distinct regions in the skulls and helped in understanding why these openings might have evolved. Finally, we used these modularity patterns and associated functional considerations to infer potential muscular associations in fossil skulls for which muscle reconstructions are very difficult to perform.

MATERIALS AND METHODS

Anatomical Framework

Skull anatomy of †*C. aguti* is well-documented in the literature (Case, 1911; Sushkin, 1928; Warren, 1961; Fox and Bowman, 1966; Bolt, 1974; Modesto, 1998; Abel et al., 2022). For coding of bone connections, we mainly rely on the study of Fox and Bowman (1966). Uncertainties related to the connection of the lacrimal to the palatine (Bolt, 1974), which we confirm to be present in a μCT-scan that was available to us (see below).

Anatomical Network Analysis

Using a walktrap algorithm, we performed an anatomical network analysis (AnNA; e.g., Rasskin-Gutman and Esteve-Altava, 2014; Esteve-Altava, 2017b; Werneburg et al., 2019; Sookias et al., 2020) for the skull of †*C. aguti* by applying the *igraph* 1.2.6 package (Csardi and Nepusz, 2006) in R (R Core Team, 2020, see also: Esteve-Altava et al., 2011; Esteve-Altava, 2017b,c). For this, an Excel sheet was created, listing the skull bones in an adjacency matrix (i.e., binary coded N × N format) with a value of 1 indicating a contact between two bones and a value of 0 for the lack of such (**Table 1**). The skull of †*C. aguti* consists of 65 bones (i.e., "nodes" in network terminology) and 322 bone contacts (i.e., "links"). The data sheet was imported into RStudio (RStudio Team, 2019) and transformed into an undirected *igraph* object to enable network depiction and calculation of community structures. We used the *cluster_walktrap* function to find community structures based on random walks with the step number being 3 (**Supplementary Table 1**). In network analyses, the resulting community structures (i.e., modules) describe subsets that share more links with each other than with the other nodes of the network, potentially representing different functional units (see discussion and Werneburg et al., 2019). Additionally, we calculated the modularity-value (Q). Q is positive when the number of contacts within the modules exceeds the expected number if all contacts were assigned randomly. Likewise, Q is negative when the number of observed contacts within a module are below the random arrangement.

TABLE 1 | Anatomical network matrix of the skull of †*Captorhinus aguti*. Connections (i.e., "1") are highlighted in blue. Please note that cells representing contacts between identical nodes (e.g., "Angular_left" vs. "Angular_left") are filled black for reading aid. For the analysis, such cells have to be coded as "0". Alterations of this matrix based on **Figures 1A,C** as well as related CSV-files can be found in the accompanying **Supplementary Material**.

	Angular_left	Angular_right	Articular_left	Articular_right	Basioccipital	Coronoid_left	Coronoid_right	Dentary_left	Dentary_right	Epipterygoid_left	Epipterygoid_right	Exoccipital_left	Exoccipital_right	Frontal_left	Frontal_right	Jugal_left	Jugal_right	Lacrimal_left	Lacrimal_right	Maxilla_left	Maxilla_right	Nasal_left	Nasal_right	Opisthotic_left	Opisthotic_right	Palatine_left	Palatine_right	Parabasisphenoid	Parietal_left	Parietal_right	Postfrontal_left	Postfrontal_right	Postorbital_left	Postorbital_right	Postparietal_left	Postparietal_right	Prearticular_left	Prearticular_right	Prefrontal_left	Prefrontal_right	Premaxilla_left	Premaxilla_right	Prootic_left	Prootic_right	Pterygoid_left	Pterygoid_right	Quadrate_left	Quadrate_right	Quadratojugal_left	Quadratojugal_right	Septomaxilla_left	Septomaxilla_right	Splenial_left	Splenial_right	Squamosal_left	Squamosal_right	Stapes_left	Stapes_right	Supraoccipital	Supratemporal_left	Supratemporal_right	Surangular_left	Surangular_right	Vomer_left	Vomer_right
Angular_left	■	0	1	0	0	0	0	1	0	0	0	0	0	0	0	0	0	0	0	0	0	0	0	0	0	0	0	0	0	0	0	0	0	0	0	0	0	0	0	0	0	0	0	0	0	0	0	0	0	0	0	0	1	0	0	0	0	0	0	0	0	1	0	0	0
Angular_right	0	■	0	1	0	0	0	0	1	0	0	0	0	0	0	0	0	0	0	0	0	0	0	0	0	0	0	0	0	0	0	0	0	0	0	0	0	0	0	0	0	0	0	0	0	0	0	0	0	0	0	0	0	1	0	0	0	0	0	0	0	0	1	0	0
Articular_left	1	0	■	0	0	0	0	0	0	0	0	0	0	0	0	0	0	0	0	0	0	0	0	0	0	0	0	0	0	0	0	0	0	0	0	0	1	0	0	0	0	0	0	0	0	0	1	0	0	0	0	0	0	0	0	0	0	0	0	0	0	1	0	0	0
Articular_right	0	1	0	■	0	0	0	0	0	0	0	0	0	0	0	0	0	0	0	0	0	0	0	0	0	0	0	0	0	0	0	0	0	0	0	0	0	1	0	0	0	0	0	0	0	0	0	1	0	0	0	0	0	0	0	0	0	0	0	0	0	0	1	0	0
Basioccipital	0	0	0	0	■	0	0	0	0	0	0	1	1	0	0	0	0	0	0	0	0	0	0	1	1	0	0	1	0	0	0	0	0	0	0	0	0	0	0	0	0	0	0	0	0	0	0	0	0	0	0	0	0	0	0	0	1	1	1	0	0	0	0	0	0
Coronoid_left	0	0	0	0	0	■	0	1	0	0	0	0	0	0	0	0	0	0	0	0	0	0	0	0	0	0	0	0	0	0	0	0	0	0	0	0	1	0	0	0	0	0	0	0	0	0	0	0	0	0	0	0	1	0	0	0	0	0	0	0	0	1	0	0	0
Coronoid_right	0	0	0	0	0	0	■	0	1	0	0	0	0	0	0	0	0	0	0	0	0	0	0	0	0	0	0	0	0	0	0	0	0	0	0	0	0	1	0	0	0	0	0	0	0	0	0	0	0	0	0	0	0	1	0	0	0	0	0	0	0	0	1	0	0
Dentary_left	1	0	0	0	0	1	0	■	1	0	0	0	0	0	0	0	0	0	0	0	0	0	0	0	0	0	0	0	0	0	0	0	0	0	0	0	1	0	0	0	0	0	0	0	0	0	0	0	0	0	0	0	1	0	0	0	0	0	0	0	0	1	0	0	0
Dentary_right	0	1	0	0	0	0	1	1	■	0	0	0	0	0	0	0	0	0	0	0	0	0	0	0	0	0	0	0	0	0	0	0	0	0	0	0	0	1	0	0	0	0	0	0	0	0	0	0	0	0	0	0	0	1	0	0	0	0	0	0	0	0	1	0	0
Epipterygoid_left	0	0	0	0	0	0	0	0	0	■	0	0	0	0	0	0	0	0	0	0	0	0	0	0	0	0	0	1	0	0	0	0	0	0	0	0	0	0	0	0	0	0	0	0	1	0	0	0	0	0	0	0	0	0	0	0	0	0	0	0	0	0	0	0	0
Epipterygoid_right	0	0	0	0	0	0	0	0	0	0	■	0	0	0	0	0	0	0	0	0	0	0	0	0	0	0	0	1	0	0	0	0	0	0	0	0	0	0	0	0	0	0	0	0	0	1	0	0	0	0	0	0	0	0	0	0	0	0	0	0	0	0	0	0	0
Exoccipital_left	0	0	0	0	1	0	0	0	0	0	0	■	0	0	0	0	0	0	0	0	0	0	0	1	0	0	0	0	0	0	0	0	0	0	0	0	0	0	0	0	0	0	0	0	0	0	0	0	0	0	0	0	0	0	0	0	0	0	1	0	0	0	0	0	0
Exoccipital_right	0	0	0	0	1	0	0	0	0	0	0	0	■	0	0	0	0	0	0	0	0	0	0	0	1	0	0	0	0	0	0	0	0	0	0	0	0	0	0	0	0	0	0	0	0	0	0	0	0	0	0	0	0	0	0	0	0	0	1	0	0	0	0	0	0
Frontal_left	0	0	0	0	0	0	0	0	0	0	0	0	0	■	1	0	0	0	0	0	0	1	0	0	0	0	0	0	1	0	1	0	0	0	0	0	0	0	1	0	0	0	0	0	0	0	0	0	0	0	0	0	0	0	0	0	0	0	0	0	0	0	0	0	0
Frontal_right	0	0	0	0	0	0	0	0	0	0	0	0	0	1	■	0	0	0	0	0	0	0	1	0	0	0	0	0	0	1	0	1	0	0	0	0	0	0	0	1	0	0	0	0	0	0	0	0	0	0	0	0	0	0	0	0	0	0	0	0	0	0	0	0	0
Jugal_left	0	0	0	0	0	0	0	0	0	0	0	0	0	0	0	■	0	1	0	1	0	0	0	0	0	0	0	0	0	0	0	0	1	0	0	0	0	0	0	0	0	0	0	0	1	0	0	0	1	0	0	0	0	0	1	0	0	0	0	0	0	0	0	0	0
Jugal_right	0	0	0	0	0	0	0	0	0	0	0	0	0	0	0	0	■	0	1	0	1	0	0	0	0	0	0	0	0	0	0	0	0	0	0	0	0	0	0	0	0	0	0	0	0	1	0	0	0	1	0	0	0	0	0	1	0	0	0	0	0	0	0	0	0
Lacrimal_left	0	0	0	0	0	0	0	0	0	0	0	0	0	0	0	1	0	■	0	1	0	1	0	0	0	1	0	0	0	0	0	0	0	0	0	0	0	0	1	0	0	0	0	0	0	0	0	0	0	0	1	0	0	0	0	0	0	0	0	0	0	0	0	0	0
Lacrimal_right	0	0	0	0	0	0	0	0	0	0	0	0	0	0	0	0	1	0	■	0	1	0	1	0	0	0	1	0	0	0	0	0	0	0	0	0	0	0	0	1	0	0	0	0	0	0	0	0	0	0	0	1	0	0	0	0	0	0	0	0	0	0	0	0	0
Maxilla_left	0	0	0	0	0	0	0	0	0	0	0	0	0	0	0	1	0	1	0	■	0	0	0	0	0	1	0	0	0	0	0	0	0	0	0	0	0	0	0	0	1	0	0	0	0	0	0	0	0	0	1	0	0	0	0	0	0	0	0	0	0	0	0	0	0
Maxilla_right	0	0	0	0	0	0	0	0	0	0	0	0	0	0	0	0	1	0	1	0	■	0	0	0	0	0	1	0	0	0	0	0	0	0	0	0	0	0	0	0	0	1	0	0	0	0	0	0	0	0	0	1	0	0	0	0	0	0	0	0	0	0	0	0	0
Nasal_left	0	0	0	0	0	0	0	0	0	0	0	0	0	1	0	0	0	1	0	0	0	■	1	0	0	0	0	0	0	0	0	0	0	0	0	0	0	0	1	0	1	0	0	0	0	0	0	0	0	0	1	0	0	0	0	0	0	0	0	0	0	0	0	0	0
Nasal_right	0	0	0	0	0	0	0	0	0	0	0	0	0	0	1	0	0	0	1	0	0	1	■	0	0	0	0	0	0	0	0	0	0	0	0	0	0	0	0	1	0	1	0	0	0	0	0	0	0	0	0	1	0	0	0	0	0	0	0	0	0	0	0	0	0
Opisthotic_left	0	0	0	0	1	0	0	0	0	0	0	1	0	0	0	0	0	0	0	0	0	0	0	■	0	0	0	0	0	0	0	0	0	0	0	0	0	0	0	0	0	0	1	0	0	0	0	0	0	0	0	0	0	0	1	0	1	0	1	0	0	0	0	0	0
Opisthotic_right	0	0	0	0	1	0	0	0	0	0	0	0	1	0	0	0	0	0	0	0	0	0	0	0	■	0	0	0	0	0	0	0	0	0	0	0	0	0	0	0	0	0	0	1	0	0	0	0	0	0	0	0	0	0	0	1	0	1	1	0	0	0	0	0	0
Palatine_left	0	0	0	0	0	0	0	0	0	0	0	0	0	0	0	0	0	1	0	1	0	0	0	0	0	■	0	0	0	0	0	0	0	0	0	0	0	0	0	0	0	0	0	0	1	0	0	0	0	0	0	0	0	0	0	0	0	0	0	0	0	0	0	1	0
Palatine_right	0	0	0	0	0	0	0	0	0	0	0	0	0	0	0	0	0	0	1	0	1	0	0	0	0	0	■	0	0	0	0	0	0	0	0	0	0	0	0	0	0	0	0	0	0	1	0	0	0	0	0	0	0	0	0	0	0	0	0	0	0	0	0	0	1
Parabasisphenoid	0	0	0	0	1	0	0	0	0	1	1	0	0	0	0	0	0	0	0	0	0	0	0	0	0	0	0	■	0	0	0	0	0	0	0	0	0	0	0	0	0	0	1	1	0	0	0	0	0	0	0	0	0	0	0	0	1	1	0	0	0	0	0	0	0
Parietal_left	0	0	0	0	0	0	0	0	0	0	0	0	0	1	0	0	0	0	0	0	0	0	0	0	0	0	0	0	■	1	1	0	1	0	1	0	0	0	0	0	0	0	0	0	0	0	0	0	0	0	0	0	0	0	1	0	0	0	1	1	0	0	0	0	0
Parietal_right	0	0	0	0	0	0	0	0	0	0	0	0	0	0	1	0	0	0	0	0	0	0	0	0	0	0	0	0	1	■	0	1	0	1	0	1	0	0	0	0	0	0	0	0	0	0	0	0	0	0	0	0	0	0	0	1	0	0	1	0	1	0	0	0	0
Postfrontal_left	0	0	0	0	0	0	0	0	0	0	0	0	0	1	0	0	0	0	0	0	0	0	0	0	0	0	0	0	1	0	■	0	1	0	0	0	0	0	0	0	0	0	0	0	0	0	0	0	0	0	0	0	0	0	0	0	0	0	0	0	0	0	0	0	0
Postfrontal_right	0	0	0	0	0	0	0	0	0	0	0	0	0	0	1	0	0	0	0	0	0	0	0	0	0	0	0	0	0	1	0	■	0	1	0	0	0	0	0	0	0	0	0	0	0	0	0	0	0	0	0	0	0	0	0	0	0	0	0	0	0	0	0	0	0
Postorbital_left	0	0	0	0	0	0	0	0	0	0	0	0	0	0	0	1	0	0	0	0	0	0	0	0	0	0	0	0	1	0	1	0	■	0	0	0	0	0	0	0	0	0	0	0	0	0	0	0	0	0	0	0	0	0	1	0	0	0	0	0	0	0	0	0	0
Postorbital_right	0	0	0	0	0	0	0	0	0	0	0	0	0	0	0	0	1	0	0	0	0	0	0	0	0	0	0	0	0	1	0	1	0	■	0	0	0	0	0	0	0	0	0	0	0	0	0	0	0	0	0	0	0	0	0	1	0	0	0	0	0	0	0	0	0
Postparietal_left	0	0	0	0	0	0	0	0	0	0	0	0	0	0	0	0	0	0	0	0	0	0	0	0	0	0	0	0	1	0	0	0	0	0	■	1	0	0	0	0	0	0	0	0	0	0	0	0	0	0	0	0	0	0	1	0	0	0	1	1	0	0	0	0	0
Postparietal_right	0	0	0	0	0	0	0	0	0	0	0	0	0	0	0	0	0	0	0	0	0	0	0	0	0	0	0	0	0	1	0	0	0	0	1	■	0	0	0	0	0	0	0	0	0	0	0	0	0	0	0	0	0	0	0	1	0	0	1	0	1	0	0	0	0
Prearticular_left	0	0	1	0	0	1	0	1	0	0	0	0	0	0	0	0	0	0	0	0	0	0	0	0	0	0	0	0	0	0	0	0	0	0	0	0	■	0	0	0	0	0	0	0	0	0	0	0	0	0	0	0	1	0	0	0	0	0	0	0	0	1	0	0	0
Prearticular_right	0	0	0	1	0	0	1	0	1	0	0	0	0	0	0	0	0	0	0	0	0	0	0	0	0	0	0	0	0	0	0	0	0	0	0	0	0	■	0	0	0	0	0	0	0	0	0	0	0	0	0	0	0	1	0	0	0	0	0	0	0	0	1	0	0
Prefrontal_left	0	0	0	0	0	0	0	0	0	0	0	0	0	1	0	0	0	1	0	0	0	1	0	0	0	0	0	0	0	0	0	0	0	0	0	0	0	0	■	0	0	0	0	0	0	0	0	0	0	0	0	0	0	0	0	0	0	0	0	0	0	0	0	0	0
Prefrontal_right	0	0	0	0	0	0	0	0	0	0	0	0	0	0	1	0	0	0	1	0	0	0	1	0	0	0	0	0	0	0	0	0	0	0	0	0	0	0	0	■	0	0	0	0	0	0	0	0	0	0	0	0	0	0	0	0	0	0	0	0	0	0	0	0	0
Premaxilla_left	0	0	0	0	0	0	0	0	0	0	0	0	0	0	0	0	0	0	0	1	0	1	0	0	0	0	0	0	0	0	0	0	0	0	0	0	0	0	0	0	■	1	0	0	0	0	0	0	0	0	0	0	0	0	0	0	0	0	0	0	0	0	0	1	0
Premaxilla_right	0	0	0	0	0	0	0	0	0	0	0	0	0	0	0	0	0	0	0	0	1	0	1	0	0	0	0	0	0	0	0	0	0	0	0	0	0	0	0	0	1	■	0	0	0	0	0	0	0	0	0	0	0	0	0	0	0	0	0	0	0	0	0	0	1
Prootic_left	0	0	0	0	0	0	0	0	0	0	0	0	0	0	0	0	0	0	0	0	0	0	0	1	0	0	0	1	0	0	0	0	0	0	0	0	0	0	0	0	0	0	■	0	0	0	0	0	0	0	0	0	0	0	0	0	1	0	1	0	0	0	0	0	0
Prootic_right	0	0	0	0	0	0	0	0	0	0	0	0	0	0	0	0	0	0	0	0	0	0	0	0	1	0	0	1	0	0	0	0	0	0	0	0	0	0	0	0	0	0	0	■	0	0	0	0	0	0	0	0	0	0	0	0	0	1	1	0	0	0	0	0	0
Pterygoid_left	0	0	0	0	0	0	0	0	0	1	0	0	0	0	0	1	0	0	0	0	0	0	0	0	0	1	0	0	0	0	0	0	0	0	0	0	0	0	0	0	0	0	0	0	■	1	1	0	0	0	0	0	0	0	0	0	1	0	0	0	0	0	0	1	0
Pterygoid_right	0	0	0	0	0	0	0	0	0	0	1	0	0	0	0	0	1	0	0	0	0	0	0	0	0	0	1	0	0	0	0	0	0	0	0	0	0	0	0	0	0	0	0	0	1	■	0	1	0	0	0	0	0	0	0	0	0	1	0	0	0	0	0	0	1
Quadrate_left	0	0	1	0	0	0	0	0	0	0	0	0	0	0	0	0	0	0	0	0	0	0	0	0	0	0	0	0	0	0	0	0	0	0	0	0	0	0	0	0	0	0	0	0	1	0	■	0	1	0	0	0	0	0	1	0	1	0	0	0	0	0	0	0	0
Quadrate_right	0	0	0	1	0	0	0	0	0	0	0	0	0	0	0	0	0	0	0	0	0	0	0	0	0	0	0	0	0	0	0	0	0	0	0	0	0	0	0	0	0	0	0	0	0	1	0	■	0	1	0	0	0	0	0	1	0	1	0	0	0	0	0	0	0
Quadratojugal_left	0	0	0	0	0	0	0	0	0	0	0	0	0	0	0	1	0	0	0	0	0	0	0	0	0	0	0	0	0	0	0	0	0	0	0	0	0	0	0	0	0	0	0	0	0	0	1	0	■	0	0	0	0	0	1	0	0	0	0	0	0	0	0	0	0
Quadratojugal_right	0	0	0	0	0	0	0	0	0	0	0	0	0	0	0	0	1	0	0	0	0	0	0	0	0	0	0	0	0	0	0	0	0	0	0	0	0	0	0	0	0	0	0	0	0	0	0	1	0	■	0	0	0	0	0	1	0	0	0	0	0	0	0	0	0
Septomaxilla_left	0	0	0	0	0	0	0	0	0	0	0	0	0	0	0	0	0	1	0	1	0	1	0	0	0	0	0	0	0	0	0	0	0	0	0	0	0	0	0	0	0	0	0	0	0	0	0	0	0	0	■	0	0	0	0	0	0	0	0	0	0	0	0	0	0
Septomaxilla_right	0	0	0	0	0	0	0	0	0	0	0	0	0	0	0	0	0	0	1	0	1	0	1	0	0	0	0	0	0	0	0	0	0	0	0	0	0	0	0	0	0	0	0	0	0	0	0	0	0	0	0	■	0	0	0	0	0	0	0	0	0	0	0	0	0
Splenial_left	1	0	0	0	0	1	0	1	0	0	0	0	0	0	0	0	0	0	0	0	0	0	0	0	0	0	0	0	0	0	0	0	0	0	0	0	1	0	0	0	0	0	0	0	0	0	0	0	0	0	0	0	■	1	0	0	0	0	0	0	0	0	0	0	0
Splenial_right	0	1	0	0	0	0	1	0	1	0	0	0	0	0	0	0	0	0	0	0	0	0	0	0	0	0	0	0	0	0	0	0	0	0	0	0	0	1	0	0	0	0	0	0	0	0	0	0	0	0	0	0	1	■	0	0	0	0	0	0	0	0	0	0	0
Squamosal_left	0	0	0	0	0	0	0	0	0	0	0	0	0	0	0	1	0	0	0	0	0	0	0	1	0	0	0	0	1	0	0	0	1	0	1	0	0	0	0	0	0	0	0	0	0	0	1	0	1	0	0	0	0	0	■	0	0	0	0	1	0	0	0	0	0
Squamosal_right	0	0	0	0	0	0	0	0	0	0	0	0	0	0	0	0	1	0	0	0	0	0	0	0	1	0	0	0	0	1	0	0	0	1	0	1	0	0	0	0	0	0	0	0	0	0	0	1	0	1	0	0	0	0	0	■	0	0	0	0	1	0	0	0	0
Stapes_left	0	0	0	0	1	0	0	0	0	0	0	0	0	0	0	0	0	0	0	0	0	0	0	1	0	0	0	1	0	0	0	0	0	0	0	0	0	0	0	0	0	0	1	0	1	0	1	0	0	0	0	0	0	0	0	0	■	0	1	0	0	0	0	0	0
Stapes_right	0	0	0	0	1	0	0	0	0	0	0	0	0	0	0	0	0	0	0	0	0	0	0	0	1	0	0	1	0	0	0	0	0	0	0	0	0	0	0	0	0	0	0	1	0	1	0	1	0	0	0	0	0	0	0	0	0	■	1	0	0	0	0	0	0
Supraoccipital	0	0	0	0	1	0	0	0	0	0	0	1	1	0	0	0	0	0	0	0	0	0	0	1	1	0	0	0	1	1	0	0	0	0	1	1	0	0	0	0	0	0	1	1	0	0	0	0	0	0	0	0	0	0	0	0	1	1	■	0	0	0	0	0	0
Supratemporal_left	0	0	0	0	0	0	0	0	0	0	0	0	0	0	0	0	0	0	0	0	0	0	0	0	0	0	0	0	1	0	0	0	0	0	1	0	0	0	0	0	0	0	0	0	0	0	0	0	0	0	0	0	0	0	1	0	0	0	0	■	0	0	0	0	0
Supratemporal_right	0	0	0	0	0	0	0	0	0	0	0	0	0	0	0	0	0	0	0	0	0	0	0	0	0	0	0	0	0	1	0	0	0	0	0	1	0	0	0	0	0	0	0	0	0	0	0	0	0	0	0	0	0	0	0	1	0	0	0	0	■	0	0	0	0
Surangular_left	1	0	1	0	0	1	0	1	0	0	0	0	0	0	0	0	0	0	0	0	0	0	0	0	0	0	0	0	0	0	0	0	0	0	0	0	1	0	0	0	0	0	0	0	0	0	0	0	0	0	0	0	0	0	0	0	0	0	0	0	0	■	0	0	0
Surangular_right	0	1	0	1	0	0	1	0	1	0	0	0	0	0	0	0	0	0	0	0	0	0	0	0	0	0	0	0	0	0	0	0	0	0	0	0	0	1	0	0	0	0	0	0	0	0	0	0	0	0	0	0	0	0	0	0	0	0	0	0	0	0	■	0	0
Vomer_left	0	0	0	0	0	0	0	0	0	0	0	0	0	0	0	0	0	0	0	0	0	0	0	0	0	1	0	0	0	0	0	0	0	0	0	0	0	0	0	0	1	0	0	0	1	0	0	0	0	0	0	0	0	0	0	0	0	0	0	0	0	0	0	■	1
Vomer_right	0	0	0	0	0	0	0	0	0	0	0	0	0	0	0	0	0	0	0	0	0	0	0	0	0	0	1	0	0	0	0	0	0	0	0	0	0	0	0	0	0	1	0	0	0	1	0	0	0	0	0	0	0	0	0	0	0	0	0	0	0	0	0	1	■

We also calculated the number of Q-modules, which describe the best mathematical threshold (red dashed line in **Figures 2**, **4–8**) to define a module. Depending on the algorithm used, this threshold might slightly shift. The Q-module is just a rough orientation to detect meaningful biological modules (see discussion in Werneburg et al., 2019; Sookias et al., 2020), and as such, the choice of the cluster optimization algorithm does not have any importance for the scope of this study (personal communication with Borja Esteve-Altava in 2021).

μCT-Scan of †*Captorhinus aguti*

For illustration of the modularity pattern (**Figures 2–8**), we used a μCT-scan of a skull of †*C. aguti* from Sam Noble Oklahoma Museum of Natural History, University of Oklahoma, Norman, OK, United States (OMNH 44816). This scan was used in a

parallel study (Abel et al., 2022) in which we describe in detail the sutures between adjacent bones to infer potential intracranial mobilities. In the μCT-scanned specimen, the following dermal bones are missing: left jugal, part of left prefrontal, left nasal, both premaxillae, most of the postparietals, and both supratemporals. The missing bones are indicated by semitransparent outlines in **Figure 2**. In other pictures of this specimen and in the skull models derived from it (**Figures 3–8**), these missing bones were not redrawn.

Skull Models

Skull models correspond to the temporal skull types defined by Abel and Werneburg (2021). For the different models of temporal skull openings, the original matrix (**Table 1**; *scutal*, i.e., anapsid type) was modified by removing particular bone connections (i.e., coding "1" replaced by coding "0"; see **Figures 1A,C,D**, Script in **Supplementary Material**). The *infrafenestral*, *bifenestral*, and *fossafenestral* skull types of Abel and Werneburg (2021) were, in the present study, divided in two sub-types each. The *nudital* and *additofenestral* skull types were not modeled within the framework of this study. For a *nudital* model, a number of bones (not just contacts) would need to be deleted, resulting in a non-comparable network as all other models in this study have a stable bone number (N). *Additofenestral* refers to multiple contacts between two adjacent bones (leaving more than one opening in between) which cannot be coded using AnNA methodology.

In the *infrafenestral-1* skull model (**Figure 3B**), which is represented by many early Synapsida [†Caseidae, †Varanopidae; e.g., Romer and Price (1940)] and some †Parareptilia (e.g., MacDougall and Reisz, 2014), the jugal/squamosal contacts of the original matrix were removed on both skull sides (i.e., "1" replaced by "0"), resulting in 318 remaining links.

In the *infrafenestral-2* skull model (**Figure 3C**), which was represented by some †Edaphosauridae and early therapsids, such as †Dinocephalia (Boonstra, 1952; Modesto, 1995; Kammerer, 2011; Lucas et al., 2018), the jugal/quadratojugal and postorbital/squamosal-contacts were removed resulting in 314 remaining links. This general pattern is also developed in many lepidosauromorphs, although their fenestra has evolved from the upper instead of the lower temporal opening (Abel and Werneburg, 2021).

In the *infrafossal* skull model (**Figure 3D**), jugal/squamosal and jugal/quadratojugal-contacts were removed, resulting in 314 remaining links. Early amniote taxa representing this morphotype are some †millerettids, †*Microleter,* and †*Eunotosaurus* (Gow, 1972; Keyser and Gow, 1981; Tsuji et al., 2010), and some "microsaurs" like †*Llistrofus* and related taxa that might also represent early amniotes (Bolt and Rieppel, 2009; Mann et al., 2019).

In the *suprafenestral* skull model (**Figure 3E**), which was represented by †*Araeoscelis* (Reisz et al., 1984), the postorbital/parietal-contact was removed, resulting in 318 remaining links.

In the *suprafossal* skull model (**Figure 3F**), supratemporal/parietal and squamosal/parietal-contacts were removed, resulting in 314 remaining links. Although not included as such by Abel and Werneburg (2021), this skull type mirrors a skull shape, which evolved in many non-amniote taxa (Holmes, 1984; Klembara et al., 2006; Reisz et al., 2009; Klembara, 2011), with the "fossa" representing the otic notch.

In the *bifenestral-1* skull model (**Figure 3G**), which was represented by the early diapsid †*Petrolacosaurus* (Reisz, 1977), postorbital/parietal and jugal/squamosal-contacts were removed, resulting in 314 remaining links.

In the *bifenestral-2* skull model (**Figure 3H**), which was likely represented by the neodiapsid †*Youngina* (Carroll, 1981), postorbital/parietal, postfrontal/parietal, and jugal/squamosal-contacts were removed, resulting in 310 remaining links.

In the *bifossal* skull model (**Figure 3I**), jugal/squamosal, jugal/quadratojugal, supratemporal/parietal, and squamosal/parietal-contacts were removed, resulting in 306 remaining links. This model represents a combination of infra- and suprafossal skull types. To our knowledge, it is not represented in any early amniote, but is a morphotype, which is well-developed in the turtle crown-group (Gaffney, 1979; Werneburg, 2012) and mammals (Novacek, 1993). As the anatomy of these animals is highly derived compared to the ancestral amniote condition (Starck, 1995; Müller, 2003; Werneburg and Maier, 2019), the model might have only little relevance to interpret the diverse skull construction in these groups (but see the section "Discussion").

In the *fossafenestral-1* skull model (**Figure 3J**) which may be represented by †*Claudiosaurus* (Carroll, 1981), jugal/squamosal, jugal/quadratojugal, and postorbital/parietal-contacts were removed, resulting in 306 remaining links.

In the *fossafenestral-2* skull model (**Figure 3K**), which may be present in the neodiapsid †*Hovasaurus* and †*Claudiosaurus* [see *fossafenestral-1* type as alternative] (Currie, 1981; Bickelmann et al., 2009), jugal/squamosal, jugal/quadratojugal, postorbital/parietal, and postfrontal/parietal-contacts were removed, resulting in 310 remaining links. This skull type is also visible in many squamates (Evans, 2008).

Muscle Reconstruction

We provide an attempt to hypothetically interpret some aspects of the functional morphology of jaw musculature in the respective skull models. Our concept was that if muscles attach to different bones of the same skull module, they are interpreted as acting as one functional entity. It has been shown that muscles are very conservatively associated to particular bones through evolution and only rarely change their general attachment sites (Diogo and Abdala, 2010; Werneburg, 2013a). Skull modules have widely been interpreted in a functional manner (Esteve-Altava et al., 2015a,b,c; Werneburg et al., 2019; Plateau and Foth, 2020). With changed osteological modularity, bone-related musculature might change its internal and external structure and functional anatomy. This could mean that the muscles could be partly or fully fused as one muscle mass and receive a common nervous signal to contract at the same time, or they could form separated muscle heads and portions with individual functional properties.

Using AnNA, Esteve-Altava et al. (2015c) have shown that different modules can be obtained when the skeletal and muscular components are modeled separately or together,

arguing against a straightforward relationship between bone modules and functional muscle groups. Despite the fact that different node numbers in an anatomical network may result in different modular integration (e.g., see our models below), this obstacle is mainly related to the premise that, in AnNA, every anatomical element—bone and muscle alike—is treated equally as just a "node" in the anatomical framework. However, bones are already very diverse in their anatomy and ontogenetic history with either their enchondral or dermal origin, resulting in altering internal structural properties (Hall, 2005). Reducing them to nodes has its limitations, but it has been shown to still be informative in anatomical network studies. Muscles are more difficult in this regard.

The conservative and tendinous attachments of muscles to particular bones are derived from neural crest cells early in development (Hall, 2009), making primary muscle-bone correspondences difficult to change through evolution. In contrast, muscles also possess a very plastic structure that functionally adapts—*via* expanded direct muscle fiber attachments to other bones—for particular biomechanical requirements. Therefore, comparing modularity of bones and modularity of muscles (Esteve-Altava et al., 2015c) should be taken with great care and detailed anatomical knowledge is needed to make sufficient correlations. A study in which muscles and bones are treated as equal structural entities (nodes) may result in an interesting overall network relationship, but with little functional meaning. Relative proportions, muscle vectors, and muscle fiber directions, among many other parameters, however, are imperative to make sufficient biomechanical reconstructions. Hence, muscle anatomy and not muscle network need to be discussed in relation to bone modularity for a sufficient functional interpretation. This exploratory, rough heuristic approach, of course, can only be speculative and needs to be tested with proper biomechanic methodology (e.g., finite element analyses: Lautenschlager et al., 2017; Ferreira et al., 2020). Nevertheless, comparative anatomical data already provide well-founded indications on a functional relationship between bone modules and muscle morphology.

For example, Werneburg et al. (2019) discussed bone modularity of five extant species and cited muscle anatomy in clear correspondence between particular bone modules and muscles. In the alligator, an expanded snout (their "red" labeled module) is related to the expanded pterygoid-musculature (Schumacher, 1973). The threefold differentiation of the external adductor muscles is closely related to the encounter of three skull modules ("green," "orange," and "red") in the temporal skull region of alligator and tuatara (Holliday and Witmer, 2007; Jones et al., 2009). Even the derived muscle anatomy of the leatherback turtle with straight jaw muscle orientation in the adductor chamber (Burne, 1905; Schumacher, 1972) directly associates with the unique skull modularity in this species ("green" and "orange"). As differentiation of the external jaw muscles in the opossum, the mammalian temporalis musculature anatomically relates to the expanded braincase module ("yellow"), whereas the complex masseter muscle used for chewing attaches to the jugal, which belongs to the snout module ("red") in this species. Even the rather simple skull modularity of the chicken corresponds to its jaw muscle anatomy (Van Den Heuvel, 1992), taking lower level network hierarchy into account (Werneburg et al., 2019).

Based on the known extant tetrapod jaw muscle diversity (e.g., Diogo and Abdala, 2010; Ziermann et al., 2019), we hypothesize at least seven distinct major jaw muscle portions to be present in the ancestral amniote condition (**Figure 3**: seven-pointed star next to each skull). These include for the external jaw adductor section: (1) musculus (m.) adductor mandibulae externus Pars profundus (AMEP), originating mainly from the parietal, (2) m. adductor mandibulae externus Pars superficialis (AMES), originating mainly from the squamosal, and (3) m. adductor mandibulae Pars medialis (AMEM), which is mainly associated with the jugal (see homology discussion in Abel et al., 2022). The internal jaw adductor section includes the following: (4) m. adductor mandibulae posterior, originating mainly from the quadrate, (5) m. pterygoideus Pars ventralis (PTV), which is mainly associated with the posterior edge and/or ventral side of the pterygoid, (6) m. pterygoideus Pars dorsalis (PTD), originating dorsally from the palatine (in addition to the pterygoid), and (7) m. constrictor internus dorsalis (CID) mainly originating from the epipterygoid. This series of seven muscular units is obviously a simplification of the actual diversity and differentiation of jaw musculature, but this generalization was necessary to fit the focus of this article and is open to revision. Muscle terminology is based on Jones et al. (2009) and Werneburg (2011).

RESULTS

Network Analysis of †*Captorhinus aguti* (Skull Type A: *Scutal*/Anapsid)

The number of contacts per bone varies from two (epipterygoid) to 13 (supraoccipital). Most bones possess three to five contacts.

TABLE 2 | Network parameters of the analyzed networks based on the definitions theoretical background as mostly summarized by Plateau and Foth (2020).

Model	C	D	K	L	Q	Q_{max}
scutal (†*Captorhinus aguti*)	0.428	0.077	322	3.663	7	0.62
infrafenestral-1	0.409	0.076	318	3.684	7	0.62
infrafenestra-2	0.430	0.075	314	3.685	7	0.62
infrafossal	0.432	0.075	314	3.697	7	0.63
suprafenestral	0.411	0.076	318	3.674	7	0.62
suprafossal	0.414	0.075	314	3.702	7	0.62
bifenestral-1	0.387	0.075	314	3.702	7	0.62
bifenestral-2	0.375	0.076	310	3.725	7	0.62
bifossal	0.416	0.074	306	3.750	7	0.62
fossafenestral-1	0.398	0.074	306	3.738	7	0.62
fossafenestral-2	0.410	0.075	310	3.715	7	0.63

For all models, N is the number of nodes (i.e., bones) and is always 65 in our models. C is the mean clustering coefficient and represents the arithmetic mean of the ratio of a node's neighbors that connect among them in a triangular manner. D is the density of connections calculated as the number of links (K) divided by the maximum number of connections possible. L is the mean shortest path length and measures the average of the shortest path length between all pairs of bones. Q is the number of calculated Q-modules. Q_{max} evaluates whether the number of modules identified are better supported than what is expected at random.

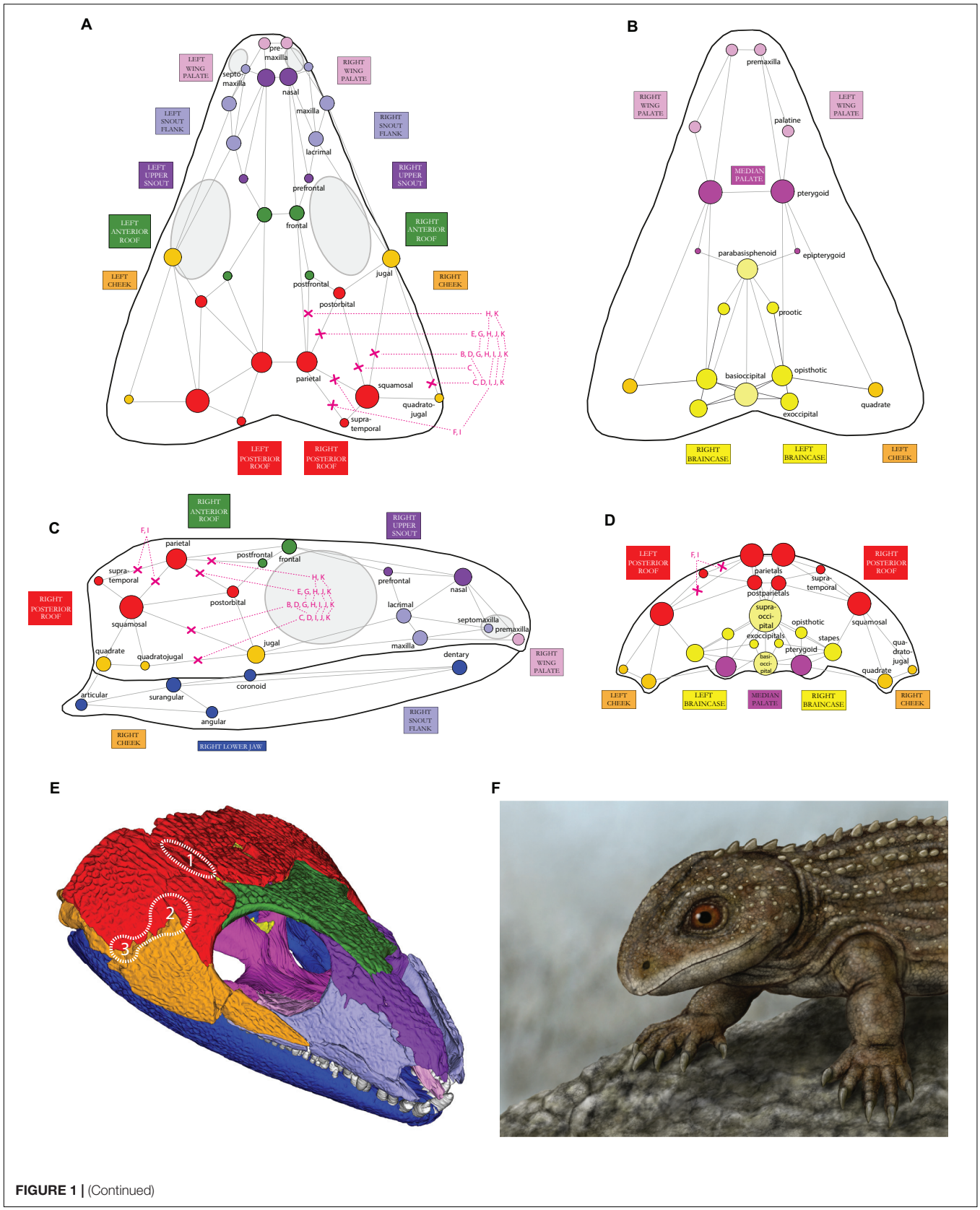

FIGURE 1 | (Continued)

FIGURE 1 | Illustration of the skull network of †*Captorhinus aguti* in **(A)** dorsal, **(B)** ventral, **(C)** lateral, and **(D)** posterior view. Only superficial bones and their connections to other bones ("links" in network terminology) are shown. The relative size of each circle (i.e., node) represents the number of links to the respective bone, incl. also non-illustrated ones (see legend inside Figure). For coding details see **Table 1**. Circles are colored according to the reconstructed cranial network modules (see **Figures 1E**, **2**). In the present study, different network models were created by cutting selected connections between particular bones, herein indicated by red "X"-symbols; letters correspond to respective models and subpanel letters in **Figure 3**). **(E)** oblique view of the 3D-reconstructed skull of †*C. aguti* with colored skull modules (see **Figures 2**, **3A** for labeling). The potential origin sites of temporal openings among early amniotes (1–3) are indicated by dotted lines (compare to **Figure 3A**: right lower corner). **(F)** Digital drawing of †*C. aguti* by paleoartist Markus Bühler (Balingen, Germany); Paläontologische Sammlung der Universität Tübingen, collection number of the drawing: GPIT-PV-112849.

In the temporal region, the squamosal is the most 'integrated' bone (eight contacts). The minimum number can be observed in the postfrontal, supratemporal, and quadratojugal (three contacts). In the conceptual framework of AnNA, integration refers to the number of connections. This is related to the concept of burden (Esteve-Altava et al., 2013a), and it has been adapted for AnNA (see Rasskin-Gutman and Esteve-Altava, 2021).

The analysis with walktrap algorithm, which has been widely used in Anatomical Network literature before, resulted in a modularity index (Q-index) of 0.625. A Q-index > 0 means that the calculated number of contacts inside a module is higher than in a random model (**Figure 2E**). Network parameters and Q-values per model are listed in **Table 2**.

Network Description for †*Captorhinus aguti* (Skull Type A: *Scutal*/Anapsid)

In addition to both left and right-side mandibular rami (dark blue in **Figures 1**–**3A**), a braincase module is present (dark yellow), and it is separated into a left and a right submodule containing prootic/stapes and opisthotic/exoccipital on each side. The unpaired elements of the braincase (light yellow)—parabasisphenoid, basioccipital, and supraoccipital—randomly appear within either one of the contralateral braincase submodules in different runs of the same analysis (see Werneburg et al., 2019 for details on that phenomenon).

The remaining major modules consist of left and right dermal bones of the "cheek," skull roof, snout, and palate regions. Inside these areas, the palate region can be divided into three modules, one left and one right-wing module (light pink), each consisting of premaxilla and palatine/vomer, and one medial palate module (dark pink). The latter plotted closer to the braincase modules (yellow) than to the palatal wing (light pink) inside the dendrogram and consists of the contralateral pterygoids and epipterygoids.

The "cheek" region lateral and posterolateral to the orbit (orange) consists of jugal and the more integrated quadrate/quadratojugal on each side. A certain relationship exists between the "cheek" and the two skull roof modules indicated by neighboring branches in the dendrogram.

The posterior roof module (red) consists of squamosal + parietal/postorbital and postparietal/supratemporal. The anterior roof module (dark green) consists of postfrontal and frontal.

In the snout, two modules can be found on each skull side. The upper snout module (dark purple) consists of prefrontal and nasal. The snout flank module (light purple) consists of maxilla and lacrimal/septomaxilla.

As for the overall network structure, the median palate modules (dark pink), together with the braincase modules (yellow), are placed in between left and right skull side modules on both skull sides functionally separating the skull in a left and right side (**Figure 2E**).

Network Analyses of the Skull Models

All ten skull models (**Figures 3B**–**K**, **4**–**8**) show seven Q-modules each (**Table 2**). We found that compared to the original skull modularity of †*C. aguti* (**Figures 2**, **3A**), the jugal, squamosal, postorbital, and postfrontal usually change their modular association when different temporal openings are modeled. Only in the original skull model, the frontal forms its own module together with postfrontal (green), but it is part of the upper snout module (dark purple) in all ten modeled skulls. Also, different to †*C. aguti*, in all ten modeled skulls, the palatal wing module (light pink) plotted closer to the snout flank module (light purple) than the latter does to the upper snout module (dark purple).

As for the overall network structure, the median palate (dark pink), together with the braincase (yellow) modules, can change their relative position in relation to the palatal wings, snout, cheek, and skull roof modules in each skull model.

In the skull model dendrograms (**Figures 4**–**8**), the original modular association of the respective bone as found in †*C. aguti* is indicated by background coloration of the respective bone name embedded in a different module coloration.

In the *infrafenestral-1* skull model, also different to the original *scutal* skull of †*C. aguti* (see **Figures 1**–**3A** vs. **Figures 3B**, **4A**), the cheek (orange) module plotted closer to the posterior roof module (red) than the latter does to the upper snout module (dark purple), as indicated by parallel white stripes in **Figure 3B**.

In the *infrafenestral-2* skull model (see **Figures 1**–**3A** vs. **Figures 3C**, **4B**), the cheek module split in two separated parts with the jugal integrated within the lateral snout module (light purple). A new module, the postocular module, is formed by postorbital and postfrontal (light green), and the cheek module (orange) is closer associated to the posterior roof module (red). Considering the overall network, the median palate module (dark pink)—together with the braincase module (yellow)—plotted closer to the skull roof (red and blue) and cheek (orange) modules than to the palatal wing (light pink) and the snout modules (light and dark pink) of both skull sides. Hence, the whole skull may be functionally separated into an anterior and a posterior half.

In the *infrafossal* skull model (see **Figures 1**–**3A** vs. **Figures 3D**, **5A**), the cheek module is split with the jugal integrated in the snout flank module (light purple). Postorbital and postfrontal are part of the posterior skull roof module

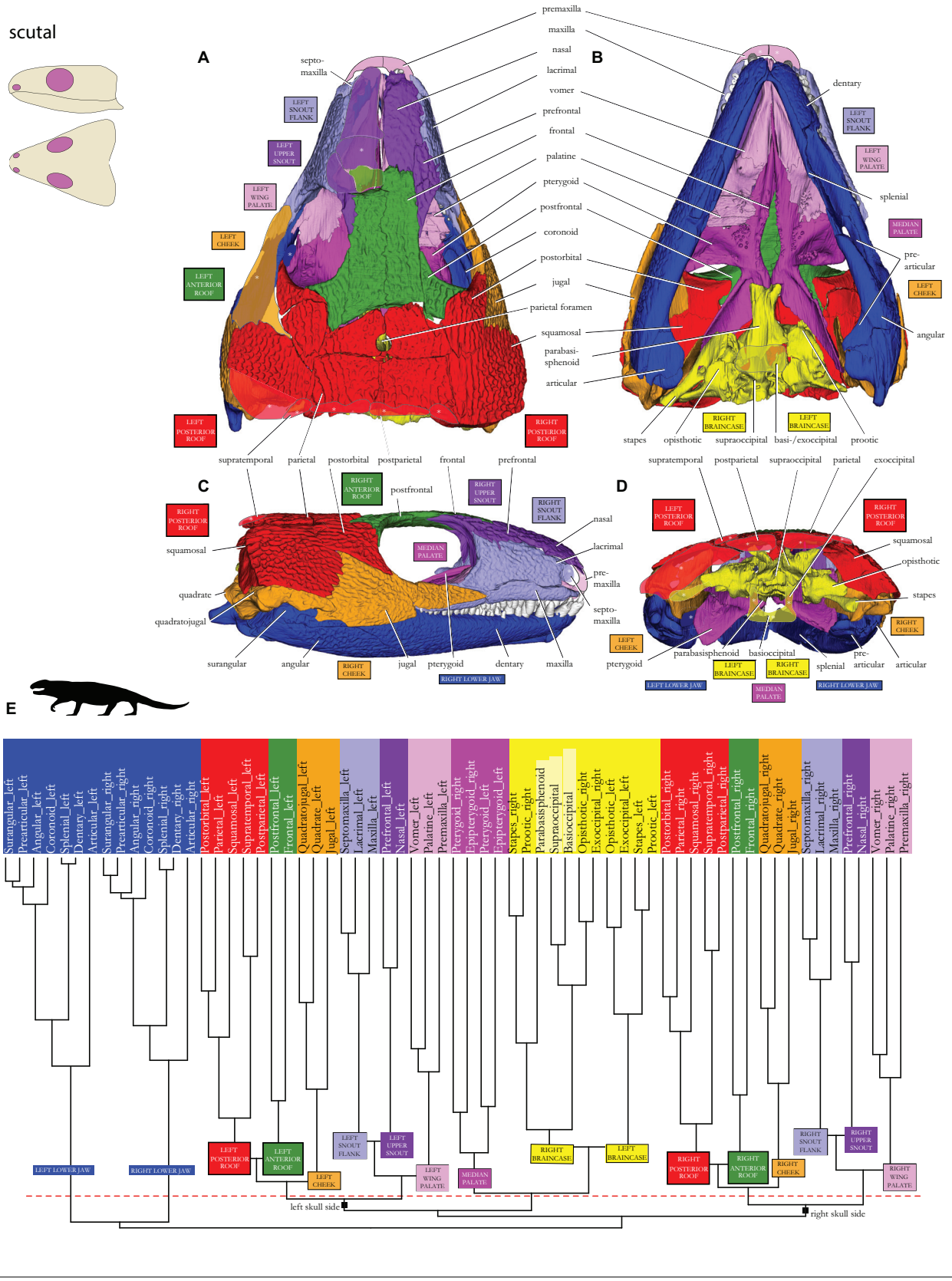

FIGURE 2 | (Continued)

FIGURE 2 | Skull network of †*Captorhinus aguti* in **(A)** dorsal, **(B)** ventral, **(C)** lateral, and **(E)** posterior view. Missing bones of the μCT-scanned skull are redrawn as rough semitransparent outlines. The dendrogram calculated during the network analysis is shown in panel **(E)**: red dashed line indicates the threshold of the Q-modules. Biologically sound morphological modules are indicated by different colors. Unpaired bones of the (yellow) braincase have no robust position in different runs of the same analysis and are shown in light yellow. Major skull network dichotomy in "right" and "left" skull sides is labeled on the basal branches (compare to double-arrows labeled as "right-left" in **Figure 3A**). Sketches of the *scutal* skull type in the upper left corner after Abel and Werneburg (2021). Silhouette in **(E)** drawn after LeBlanc et al. (2018).

(red). Similar to the *infrafenestral-2* model, the median palate module (dark pink), together with the braincase module (yellow), functionally separates the whole skull in an anterior and a posterior half.

In the *suprafenestral* skull model (see **Figures 1**–**3A** vs. **Figures 3E**, **5B**), the squamosal, which originally belonged to the posterior skull roof module (red), is now part of the cheek region (orange). The jugal, which originally belonged to the cheek module, is part of the snout flank module (light purple).

The *suprafossal* skull model (see **Figures 1**–**3A** vs. **Figures 3F**, **6A**) is characterized by an expansion of the posterior skull roof module (red), which now also includes postfrontal and all three (originally orange) cheek bones: quadrate, quadratojugal, and jugal.

The *bifenestral-1* skull model (see **Figures 1**–**3A** vs. **Figures 3G**, **6B**) shows the same patterns as the *infrafenestral-1* model (see **Figures 3B**, **4A**)

In the *bifenestral-2* skull model (see **Figures 1**–**3A** vs. **Figures 3H**, **7A**), postfrontal and postorbital form a new postocular module (light green) that is related to the cheek (orange) and to the posterior skull roof (red) modules.

In the *bifossal skull* model (**Figures 1**–**3A** vs. **Figures 3I**, **7B**), the jugal becomes part of the lateral snout module (light purple). The posterior skull roof module (red) has expanded and integrates the two remaining "cheek elements", quadrate and quadratojugal, along with the postfrontal. Considering the overall network, the median palate module (dark pink)—together with the braincase module (yellow), are closely placed in between the posterior skull roof modules of both skull sides (red), functionally separating the whole skull in an anterior and a posterior half. The anterior half is formed by the palatal wing modules (light pink) and the snout modules (light and dark purple) of both skull sides.

In the *fossafenestral-1* skull model (see **Figures 1**–**3A** vs. **Figures 3J**, **8A**), postfrontal and postorbital form a new, postocular module (light green) that plotted closer to the posterior skull roof (red) module than to the cheek module (orange). The cheek module is split with the jugal, which is now integrated inside the snout flank module (light purple). Median palate modules (dark pink), together with the braincase modules (yellow), are closer related to skull roof (red and light green) and cheek (orange) modules of both skull sides than to the remaining skull modules, again functionally separating the skull in an anterior and a posterior half.

Like in the *fossafenestral-1* skull model (**Figures 3J**, **8A**), the *fossafenestral-2* skull model (see **Figures 1**–**3A** vs. **Figures 3K**, **8B**) shows a postocular module. In this model, however, cheek (orange) and posterior skull roof (red) module plotted closer to each other than both do to the postocular module (light green) (see white parallel stripes in the figure). Like in the *fossafenestral-1* type, the cheek module is also split with the jugal being integrated inside the snout flank module (light purple). Also, as in this skull type, the *fossafenestral-2* skull is functionally separated in an anterior and a posterior half. However, the median palate module (dark pink)—together with the braincase module (yellow)—is even more strongly integrated between roof and cheek modules (red, blue, and orange) of both skull sides.

Muscle Reconstruction

The reconstructed jaw muscle associations directly correspond to the modular pattern of each skull model (i.e., seven-pointed star in **Figure 3**). In the original skull of †*C. aguti* (*scutal*/anapsid type, **Figure 3A**), the following joined muscles are reconstructed and interpreted to act as functional entity: AMEP with AMES (belonging to the red module), CID with PTV (dark purple), and AMP with AMEM (orange). The identity of AMP of either belonging to the internal or external section of the jaw musculature appears to change among taxa based on altering ontogenetic pathways (Rieppel, 1987; summarized by Werneburg, 2011). As such, an association of muscle portions usually assigned to the internal (AMP) or external (AMEM) section of the jaw adductor is not deceptive.

In †*C. aguti*, the pterygoid teeth reach far posteriorly on the ventral surface (**Figure 2B**), preventing broad insertion of PTV. Whether PTV was actually developed as a small muscle portion or whether it was just a small muscle head inserting on the posterior edge of the pterygoid cannot be determined (see discussion by Witzmann and Werneburg, 2017). A PTD could have been partly associated with CID/PTV—as indicated by the half-connected points of the star in **Figure 3A**—as the related bone module (light pink) was not as strongly integrated in the snout modules as both snout modules are into each other (light and dark purple: close association indicated by two parallel white lines in **Figure 3A**).

Muscular associations are different in all of our skull models (**Figures 3B–K**). In the *infrafenestral-1* model (**Figure 3B**), with the anterior expansion of the posterior skull roof module (red), the following muscular associations are hypothesized based on the modular pattern of related bones: AMES with AMEP (red), AMP with AMEM (orange), CID with PTV. AMP and AMES could had been partly connected due to the related modules showing a strong relation to each other.

In the model *infrafenestral-2* (**Figure 3C**), with the formation of a postocular module (light green) and the integration of the jugal into the snout flank (light purple), the following associations are hypothesized: AMES with AMEP (red), CID with PTV. Based on close modular associations, AMP could be partly related to AMES/AMAP, and AMEM to PTD.

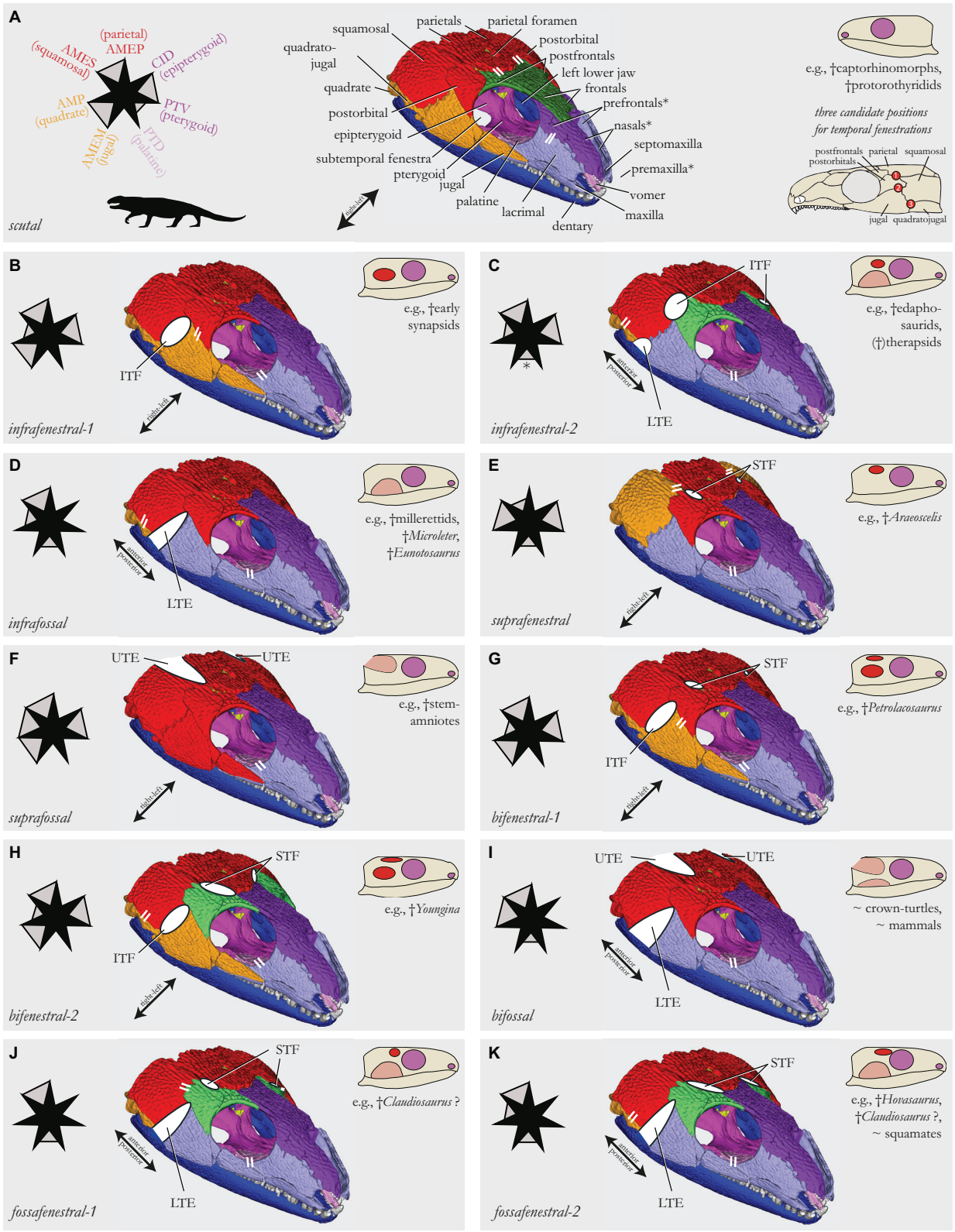

FIGURE 3 | (Continued)

FIGURE 3 | Skull network illustrations of models that simulate different temporal skull morphotypes (see sketches in each subfigure) found in early amniote evolution [based on Abel and Werneburg (2021); *nudital* and *additofenestral* skull types were not possible to model, see text]. The skull of †*Captorhinus aguti* **(A)** was used as model template. Skull models are shown in an anterior dorsolateral view **(B–K)**. Parallel white stripes indicate a closer network relationship of the connected modules when compared to other modules in the anterior (snout) or posterior (temporal) skull half, respectively (compared to dendrograms in **Figures 2E**, **4**–**8**). Modeled temporal fenestrae are shown as white full-ellipses, temporal excavations as white half-ellipses. Star-schemes for each model indicate the differentiation of muscle portions (i.e., the points of the star) inside the jaw adductor chamber [see legend in panel **(A)**; the listed bones serve as major origin sites of these muscle portions; letter coloration based on skull modules]. Muscle portions that putatively act as a joined entity are connected by gray filling between star jags; full filling means that the muscles originate from the same skull module (e.g., red), half filling means that the modules, to which the muscle portions attach, are closely associated to each other in the global anatomical network (compared to dendrograms of **Figures 2E**, **4**–**8**). AMEM, musculus (m.) adductor mandibulae Pars medialis; AMEP, m. adductor mandibulae Pars profundus; AMES, m. adductor mandibulae Pars superficialis; AMP, m. adductor mandibulae posterior; ITF, infratemporal fenestra; LTE, lower temporal excavation; PTD, m. pterygoideus Pars dorsalis; PTV, m. pterygoideus Pars ventralis (perhaps not yet differentiated in †*C. aguti*); STF, supratemporal fenestra; UTE, upper temporal excavation.

In the *infrafossal* model (**Figure 3D**), with the integration of the jugal into the snout flank (light purple), the following association is hypothesized: AMES with AMEP (red). Based on close modular associations, AMP could be partly related to AMES/AMAP, and AMEM to PTD. CID is considered more separate from PTV, because in the skull, which is differentiated in an anterior and a posterior part in overall network composition (**Figure 5A**), the CID-associated epipterygoid might serve a key role in functional anatomy (see section "Discussion").

In the *suprafenestral* model (**Figure 3E**), with the integration of the jugal to the snout flank (light purple) and the integration of the squamosal into the cheek module (orange), following associations are hypothesized: AMES with AMP (orange), CID with PTV (dark purple). AMEP (red) and AMES/AMP (orange) might be partly associated, similar to AMEM (light blue) and PTD (light pink) based on close relationship of the related skull modules.

In the *suprafossal* model (**Figure 3F**), with the expansion of the posterior skull roof module above the whole temporal region (red), the following associations are hypothesized: AMEP with AMES, AMP, and AMEM (red), and CID with PTV (dark pink).

The *bifenestral-1* model (**Figure 3G**) shows the same patterns as the *infrafenestral-1* model (**Figure 1B**).

In the *bifenestral-2* model (**Figure 3H**), with the formation of a postocular module (light green), the following associations are hypothesized: AMEP with AMES (red), AMP with AMEM (orange), and CID with PTV (dark pink). Partial relationship might exist between AMP (orange) and AMES (red).

In the *bifossal* model (**Figure 3I**), with the expansion of the posterior skull roof module to the cheek and postocular region (red) and with integration of the jugal to the snout flank (light purple), the following associations are hypothesized: AMEP with AMES and AMP (red). Partial relationship might exist between AMEM (light purple) and PTD (light pink).

In the *fossafenestral-1* and *-2* models (**Figures 3J–K**), with the formation of a postocular module (light green) and the integration of the jugal into the snout flank (light pink), the following associations are hypothesized: AMEP and AMES (red), and a partial association between AMEM (light purple) and PTD (light pink).

DISCUSSION

Significance of the Anatomical Network Approach

Using the anatomical network approach, we detected seven distinct anatomical modules on each skull side of †*C. aguti* (**Figures 1**–**3A**). These include cheek (orange in Figures), anterior (green) and posterior (red) skull roof, palate wing (light pink), upper snout (purple), snout flank (light blue), and braincase (yellow) modules. In addition, there is a median palate module (dark pink). By modeling changes in skull network composition of †*C. aguti* to mimic skull types of other early amniotes, alterations in the number and fundamental rearrangements in the respective bone composition of skull modules occur, illustrating the sensitivity of the anatomical network approach.

When trying to interpret the functional meaning of module composition, one needs to keep in mind the methodological basis of network analysis which considers as data source just the information on presence and absence of bone connections (1/0 codification) but neglects any detailed morphological characteristic such as suture type, thickness, and gross anatomy of bones. Each level of morphological organization, however, conveys different information, and to understand processes in evolution, each may first be treated separately (Rasskin-Gutman, 2003) before expanding toward a more holistic view on anatomical tissue integration (Maier and Werneburg, 2014). The functional meaning of skull modules, of course, has to be handled with care, and discussion always requires a thorough consideration of other morphological aspects known for the taxon in question and comparable organisms (Werneburg et al., 2019).

Functional considerations of skull anatomy cannot be performed without proper knowledge on muscle anatomy, which is usually barely described in the literature for extant taxa and usually misses relevant information of muscle fiber-compositions and orientations and tendinous components. For extinct taxa, only gross morphology of musculature can be reconstructed on a rough anatomical level, mainly based on phylogenetic bracketing and by considering indications of possible attachment sites on bones (Witzmann and Werneburg, 2017). Nevertheless, anatomical network methodology has been proven to provide basis for reasonable functional conclusions and new hypotheses (Esteve-Altava et al., 2013a,b, 2015a;

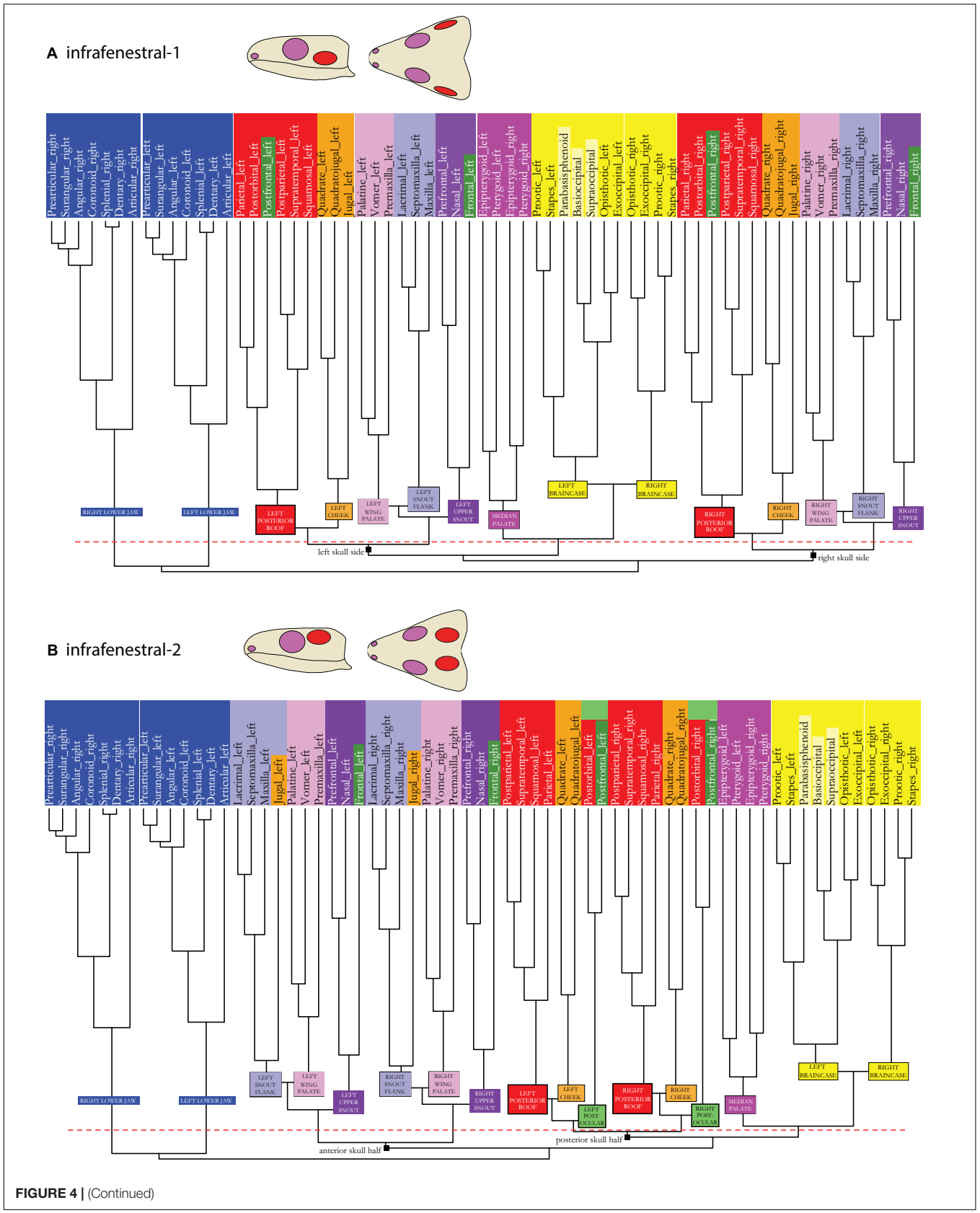

FIGURE 4 | (Continued)

FIGURE 4 | Dendrogram of the skull network of **(A)** the *infrafenestral-1* and **(B)** the *infrafenestral-2* skull types. Compare to caption of **Figure 2E**. The basal dichotomies in left and right skull side **(A)** or in an anterior and a posterior skull part **(B)** are indicated in the dendrogram.

Rasskin-Gutman and Esteve-Altava, 2014; Diogo et al., 2015; Molnar et al., 2017; Lee et al., 2020; Plateau and Foth, 2020; Sookias et al., 2020).

Rasskin-Gutman (2003) provided a first attempt to study skull modularity in relation to temporal openings and found, by comparing nine different tetrapod skulls, that the orbit is surrounded by a rather simple modular arrangement with one element attaching to at least three other adjacent elements. In contrast, the temporal region is rather complex with bones having five or six contacts to other bones which are, eventually, surrounded by bones with triangular connections again. He also found that the snout is less variable in regard to network connections than the postorbital region, which overlaps with the known morphological and trophic diversity of extant taxa (see also Werneburg et al., 2019). As such, the complexity of the anatomy network might provide a reasonable source to understand patterns of functional morphology, in which jaw muscle anatomy it taken into account.

Cranial Kinesis in †*Captorhinus aguti* With Respect to Skull Modularity

Studying the suture anatomy and thickness of dermatocranial bones, Abel et al. (2022) discussed cranial kinesis in †*C. aguti*. The authors discussed metakinesis—a movement of the temporal dermatocranium together with the snout relative to the braincase (Iordansky, 1990)—to be present between parietal/postparietal and supraoccipital and between squamosal and opisthotic. In fact, a metakinetic joint was likely widespread among early amniotes (Carroll, 1969; Gow, 1972; Bramble and Wake, 1985; Iordansky, 1990). This is further supported by the modularity pattern detected in the present study, in which the braincase elements (yellow) are separated from all other skull modules, including the posterior skull roof module with the squamosal (red) and the anterior skull roof module with the frontal (dark green).

Squamosal and parietal are plotted closely within the posterior skull roof module (red). Consequently, a representation of the ancestral "crossopterygian hinge line" (Kemp, 1980) between squamosal and more dorsal bones of the skull roof, which temporarily might have been opened posteriorly as an otic notch in early tetrapods (but see Panchen, 1964), cannot be postulated herein. However, the suture between both elements in †*C. aguti* is not very strong (Abel et al., 2022), which might be mirrored in the even closer modular relationship of the parietal to the postorbital in our reconstruction (**Figure 2E**).

Interdigitation and great thickness of the frontoparietal suture most likely prevented true joint and elasticity-based (sensu Natchev et al., 2016) mesokinetic movement in between the skull roof elements that otherwise could have been moved against each other by the contraction of m. adductor mandibulae externus Pars profundus (AMEP) (Abel et al., 2022). Frontal (dark green) and parietal (red), however, belong to different modules in the skull illustrating that clear modular distinctions between bones must not necessarily indicate a kinetic association of them. Nevertheless, mesokinesis, as widely found in squamates (Iordansky, 2011), might be an evolutionary result from the intersection between the posterior skull roof module (red) and the more anterior dorsal skull bones (dark green and dark purple) already established in an early amniote like †*C. aguti*. In fact, all models with temporal openings (**Figures 3B–K**) show a clear distinction between the posterior skull roof module (red) and the upper snout modules, the latter of which always includes the frontal bone (dark purple), and as such, this condition then might further favor mesokinetic evolution.

A pleurokinetic joint—a mediolateral movement of the quadrate relative to the rest of the skull (Evans, 2008)—was present in †*C. aguti* between quadrate on the one hand and pterygoid, quadratojugal, and squamosal on the other hand, being enabled by the contraction of musculus (m.) adductor mandibulae posterior (AMP) (Abel et al., 2022). In the present modularity study, the quadrate of †*C. aguti* belongs to the cheek module (orange), clearly separated from pterygoid (dark pink) and squamosal (red). Only the quadratojugal (in addition to the jugal) is found to share a modular identity with the quadrate. Apparently, a shared modular identity does not necessarily preclude internal kinetics within a module. The reportedly thin bones of the cheek region (Fox, 1964) likely permitted a certain elasticity of that region, driven by contraction of m. adductor mandibulae Pars medialis (AMEM; sensu Abel et al., 2022) and Pars superficialis (AMES).

Kinesis within the snout (prokinesis and rhynchokinesis) was certainly not possible based on the strong suturing of the snout bones (maxilla, lacrimal, and jugal). Bite forces were likely absorbed by the more elastic sutures in the more dorsal snout bones, namely, between nasal and prefrontal (Abel et al., 2022). Herein, an absorption of biting forces in the upper snout is further supported by the presence of an upper snout module (dark purple) ventrally separated from the snout flank (light purple). The frontal and prefrontal contact is characterized by a simpler (although still thick) suture, that could indicate that this region is less effected by compressional forces (sensu Abel et al., 2022).

A mobility of the palate, a feature that first evolved toward Amniota (Carroll, 1969), was likely possible in †*C. aguti* given the small relative thickness and simple suture types between vomer, palatine, and pterygoid. Also, a potential kinetic articulation between palatine and maxilla was present (Fox and Bowman, 1966; Abel et al., 2022). The latter pattern is mirrored in the modularity of the palate with the elastic vomer and palatine forming a module together with the premaxilla, which functionally belongs to the palatal wing (light pink).

Pro- and retraction of the palate in relation to the rest of the skull might have been enabled by the pterygoid-associated epipterygoid as a basicranial articulation of the

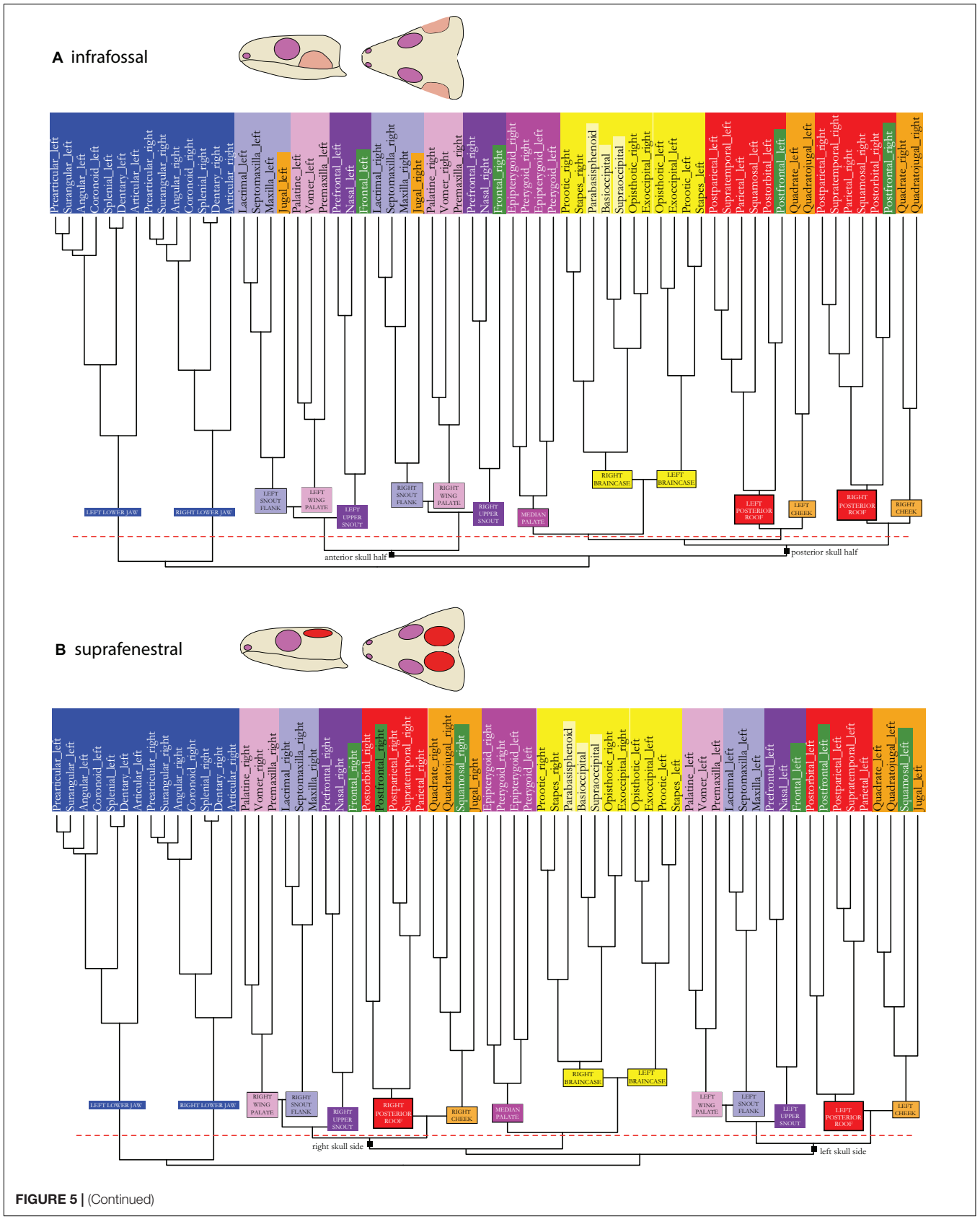

FIGURE 5 | (Continued)

FIGURE 5 | Dendrogram of the skull network of **(A)** the *infrafossal* and **(B)** the *suprafenestral* skull types. Compare to caption of **Figure 2E**. The basal dichotomies in left and right skull sides **(A)** or in an anterior and a posterior skull part **(B)** are indicated in the dendrogram.

epipterygoid to the braincase and a kinetic articulation between palatine and maxilla were present (Abel et al., 2022). Pterygoid and epipterygoid together form a distinct module by their own reflecting their positional intersection between many skull modules and their various moveable and non-moveable articulations with other elements.

In sum, the observations in †*C. aguti* illustrate a relatively good association of cranial kinesis and skull modularity, although both relative thickness and suture type between adjacent bones require a balanced consideration of functional skull morphology (Esteve-Altava, 2017a).

†*Captorhinus aguti* and the Origin of Temporal Skull Openings in Amniotes

It has been repeatedly discussed that particularly thin skull areas are prone to reduction as little forces are acting on these regions (e.g., Jaeckel, 1902; Case, 1924; Romer and Price, 1940; Fox, 1964). Temporal skull openings appear to develop particularly at the intersection between three adjacent bones (Frazzetta, 1968; Kuhn-Schnyder, 1980). Taking †*Captorhinus aguti* as a model, Abel et al. (2022) highlighted the intersections of (1) postorbital, squamosal, and parietal, of (2) jugal, squamosal, and postorbital, and of (3) jugal, squamosal, and quadratojugal as candidate areas for temporal openings in early amniote evolution (see also image with numbers in **Figures 1E, 3A**). In the following, we use the modularity pattern in †*C. aguti* to infer potential areas for temporal openings.

(1) As mentioned above, the ancestral "crossopterygian hinge line" between squamosal and more dorsal skull roof bones could not be recovered in †*C. aguti* herein, because both elements belong to one single module (red). This could indicate that the structural lability of the "crossopterygian hinge line" was stabilized in early amniotes by a close integration of both elements. Nevertheless, †*C. aguti* is still characterized by weak suturing between squamosal and parietal (Abel et al., 2022). As such, this suture could have served as potential origin area of the supratemporal opening later on in evolution ("1" in **Figures 1E, 3A**), as visible in diapsid species, or even - as discussed by Kemp (1980) - as an area that opened to allow dorsal expansion of the infratemporal region in therapsid synapsids.

(2) The modular distinction between jugal (orange) and postorbital/squamosal (red), together with the edge-like geometry of this intersection, makes this area a preferred candidate for the widely occurring infratemporal opening ("2" in **Figures 1E**, **3A**). Force vectors of AMEM (orange) and AMEP (red) musculature, pointing in different directions, will have further triggered the emergence of that opening.

(3) Similar to (2), the relatively rarely occurring opening between quadratojugal, jugal, and squamosal ("3" in **Figures 1E**, **3A**) might mainly result from the intersection of two modules (red and orange), specific arrangements of surrounding musculature (i.e., AMEM, AMES), plus the structural dissolution of the edge-like geometry of this intersection. This edge, however, is less pointy than in (2), which might explain the rare occurrence of this opening. Whether the infratemporal openings (2) and (3) actually have separated phylogenetic origins and whether they emerge from one unique opening or unite to one opening in the respective taxa cannot be evaluated herein. We rather expect the whole sutural area between squamosal and jugal to serve as potential *region* for any infratemporal opening (**Figure 1E**: indicated by white dashed line around "2" and "3"), depending on species-specific configurations and compositions of the surrounding temporal bones. In species with reduced quadratojugal, for example, a more dorsal position of the opening is common (Kemp, 1982).

Rasskin-Gutman (2003) distinguished between "active and passive fenestrae" in the vertebrate skull. Whereas "active" ones between three adjacent bones (i.e., foramina) cannot close because they surround other ("active") tissue like nerves or vessels, the "passive" ones in between four or more bones remain stable ("passive") along a phylogenetic lineage as long as no heterochronic event (relative growth in ontogeny) closes that opening. As such, to better understand transformations in temporal architecture, a greater focus on ontogenetic studies (Rieppel, 1984; Haridy et al., 2016; Werneburg, 2019; Lee et al., 2020) are urgently needed in the future.

As extensively discussed by Abel et al. (2022), taking †*C. aguti* as a model for early temporal skull evolution in amniotes has its limitations given the already derived skull anatomy of this species compared to the assumed ancestral amniote. Nevertheless, indications from their study on suture anatomy plus the present support of modularity patterns provide a reasonable chain of argumentations to understand the origin of temporal openings in early amniotes. To further explore such evolutionary modifications, the modeling of different skull types, as performed in this study, provides a valuable framework to examine the complexity of cranial changes associated with temporal fenestrations.

Modeling Temporal Openings

Modeling temporal openings into the skull network of †*C. aguti* of course comes with limitations. Obviously, there are no taxa in the fossil record that correspond to a fenestrated variant of †*C. aguti*. Skull proportions along with bone number, suture lengths, and suture anatomy can drastically differ in early amniote species with temporal openings when compared to †*C. aguti*. At this point, the above-mentioned simplification of the anatomical network methodology might actually be of a certain advantage as skull proportions and suture morphology are not considered in that approach.

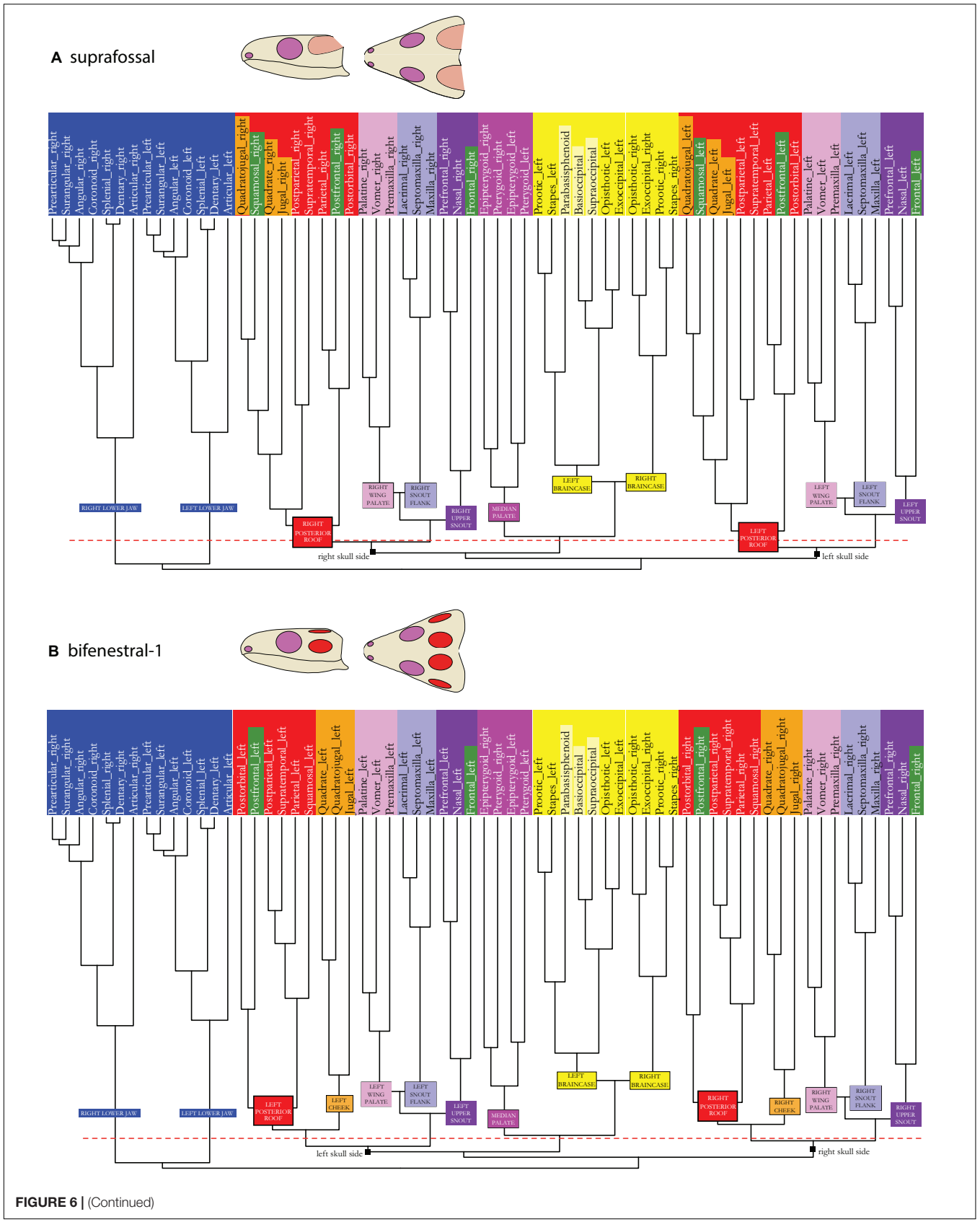

FIGURE 6 | (Continued)

FIGURE 6 | Dendrogram of the skull network of **(A)** the *suprafossal* and **(B)** the *bifenestral-1* skull types. Compare to caption of **Figure 2E**. The basal dichotomies in left and right skull sides are indicated in the dendrogram.

In our models, we kept the number of skull bones and their general connectivity stable to enable direct comparisons between the †*C. aguti* network and the skull models derived from them. However, some bones, postparietal, supratemporal, and septomaxilla in particular (Gaffney, 1990; Koyabu et al., 2014; Higashiyama et al., 2021), are known to get reduced through amniote evolution (Esteve-Altava et al., 2013b). Nevertheless, most early amniotes, which are the focus of our study, still have these bones preserved. Moreover, bones usually do not get lost as such. Particularly, during ontogeny, their ossification centers generally fuse to 'larger' bones (Klembara et al., 2002; Polachowski and Werneburg, 2013; Koyabu et al., 2014; Werneburg et al., 2015; Smith-Paredes et al., 2018), and coding their presence and ancestral connection to "larger" bones, argumentally, can be judged as a reasonable methodological approach to retain comparability in this study.

In our opinion, the only major limitation of our model-comparison is the fact that some early amniotes still have a tabular bone and an ectopterygoid. Most captorhinids, including †*C. aguti*, lack them (e.g., Clack and Carroll, 1973; Berman and Reisz, 1986; Dodick and Modesto, 1995; Müller and Reisz, 2005) and they were, hence, not modeled herein. In this regard, we again highlight the hypothetical character of any model in this study to understand the basic structural relationships inside the amniote skull.

Anatomical network analysis with actual species instead of models should be performed in the future to test and specify our initial attempts. These species would need a comparable observation of suture anatomy (Jones et al., 2011) and muscle reconstruction before, as has been done for †*C. aguti* (Abel et al., 2022). Fossil preservation of early amniotes, however, is poor in many cases and bone connections can be hard to reconstruct.

Evolutionary Changes in Functional Skull Morphology Induced by Temporal Openings

The Palate Is Functionally Associated With Changes in the Temporal Skull Region

The modeling of temporal openings into the anapsid skull (**Figure 3A**; *scutal* skull after Abel and Werneburg, 2021) results in a number of changes in the composition of skull modules. The most frequent skull opening in early amniotes was an infratemporal fenestra (ITF in **Figure 3**), modeled as disconnection between jugal and squamosal herein (**Figures 1A,C**: B-cut; *intrafenestral-1* type). Whereas the modularity of the manipulated temporal skull coverage stays mainly unaltered, the snout flank (light purple) becomes more integrated with the palate wing (light pink) (**Figures 3B**, **4A**). This might be interpreted by a more posterior and, through a shorter lever arm, by a more powerful processing of food items in the center of the mouth. In fact, early synapsids are usually considered to have fed on hard food items associated with carnivore or herbivore feeding (Kemp, 1982; Werneburg, 2019). To process those, they might have been selected for a more powerful jaw adductor musculature. As illustrated herein (seven-pointed star in **Figure 3B**), this might have been permitted by up to four muscle portions acting in union, i.e., AMP, AMEM, AMES, and AMEP.

A close integration of the snout flank (light purple) and the palate wing (light pink) is actually found in all modeled skulls, indicating a general adaptation to different food processing in amniotes when compared to their ancestors with further specifications by positional alteration or addition of opening(s) in the respective taxa. In therapsid synapsids, for example, a strong integration of snout and palate is related to the formation of a secondary palate introduced by neonatal lactation (Maier, 1999) along with a more effective carnivore and herbivore feeding behavior, which required a strengthened palatal region. This change in therapsids was associated with a dorsal shift and expansion of the infratemporal fenestra (ITF) and a lower temporal excavation (LTE) (Abel and Werneburg, 2021). Change in jaw muscle integration might be correlated with the observed bone modularity. With the development of a masseter muscle (i.e., AMEM-related following the argumentation of Abel et al., 2022) and an associated loss of the quadrate from the temporal region (i.e., it moves as incus to the middle ear; Werneburg, 2013b), chewing behavior emerged in cynodont therapsids (Abdala and Damiani, 2004). The adjusted side and inward movements during chewing could actually be mirrored in the postulated functional union of AMEM (masseter) and PTD musculature (asterisk in **Figure 3C**). The greater stability of the skull by formation of a secondary palate to withstand higher suckling and biting forces is also associated with the successive integration of the epipterygoid (as alisphenoid) to the secondary braincase wall toward Mammalia (Maier, 1989, 1999). The certain independency of the median palate module (dark pink) to which the epipterygoid belongs in the anatomical network might have been, in this case, a precondition to uncouple this element from the palate.

The anatomical network modularity of an extant omnivorous mammal (*Didelphis virginiana*: Werneburg et al., 2019), which resembles the *infratemporal-2* skull type, shows a certain similarity to our *infratemporal-2* model in the way that the jugal and palatal region belong to the same module. Noteworthy, the fusion of the orbit with the infratemporal opening in that species has major impact on the modularity of the anterior and posterior dermal skull region. The latter is forming one consistent module with the braincase. This becomes obvious when comparing the results for *D. virginiana* to the pattern observed in primates, in which the postorbital bar is present and the frontal changes its modular association (Esteve-Altava et al., 2015a,c). Changing just one connection in the skull has major impact on general modular compositions.

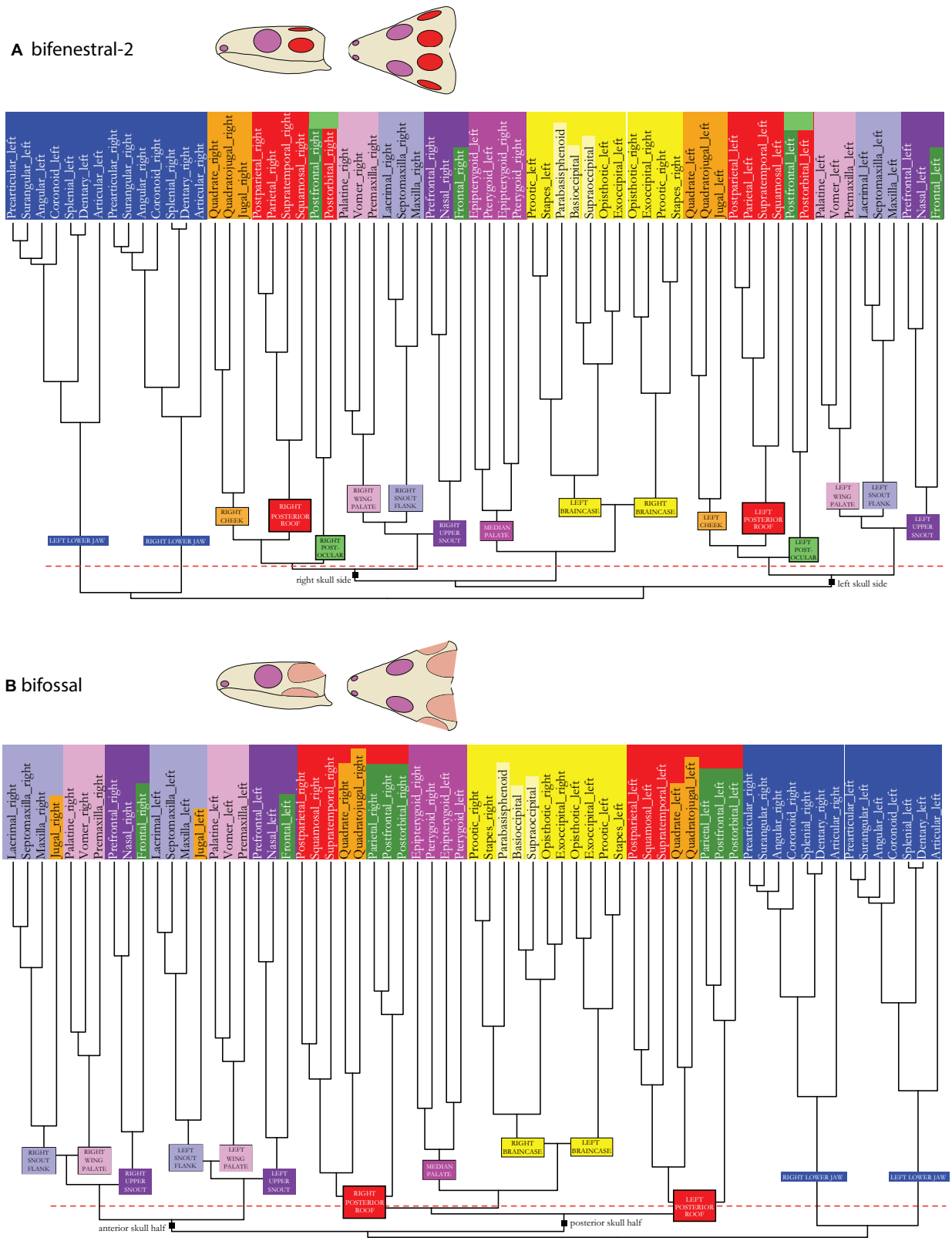

FIGURE 7 | (Continued)

FIGURE 7 | Dendrogram of the skull network of **(A)** the *bifenestral-2* and **(B)** the *bifossal* skull types. Compare to caption of **Figure 2E**. The basal dichotomies in left and right skull sides (A) or in an anterior and a posterior skull part (B) are indicated in the dendrogram.

Convergent Evolution of Stronger Bite in Terrestrial Habitats

The modeling of a lower temporal excavation (LTE) in the skull (**Figure 3D**; *infrafossal* type) results in the integration of the jugal into the snout flank module (light purple), suggesting a more powerful initial capture of hard food items anteriorly in a robust snout, possibly imaginable for †*Eunotosaurus africanus* (Watson, 1914; Keyser and Gow, 1981) and other extinct taxa with similar temporal skull arrangement (e.g., †*Llistrofus*, †*Microleter*, †*Millerosaurus*, †*Milleropsis*). Further food manipulation more posterior in the mouth, for instance by positioning of the food item before swallowing using pterygoid teeth (Gow, 1997), might have been more complex. With the formation of a lower temporal excavation, the overall network integrity falls into an anterior and a posterior skull part (double-headed arrows in **Figures 3C,D**), which could hint to a more important role of the epipterygoid bone (dark pink) as pivot point between them, as indicated by a more independent related CID-musculature in our muscle reconstruction.

The presence of only a supratemporal fenestra (STF), like in the early diapsid †*Araeoscelis,* resulted in a dorsal expansion of the cheek module toward squamosal (orange) (**Figure 3E**; *suprafenestral* type). †*Araeoscelis* "exhibits a suite of unusual cranial features resulting in a massive, sturdily constructed skull, which is interpreted as an adaptation to a specialized diet that probably included invertebrates protected by heavy exoskeletons" (Reisz et al., 1984, p. 57). To enable this strong bite, according to the detected modularity pattern, AMES, AMP, and AMEP on the one hand, and AMEM and PTD on the other hand might have separately worked as unions. The comparison with heavy-snouted *infrafossal* taxa from the Permian (Abel and Werneburg, 2021) shows that different "experimentations" of temporal region anatomy were performed in early amniote evolution to exploit similar food resources that now became available in fully terrestrial habitats.

The presence of an upper temporal excavation (UTE) (**Figure 3F**, *suprafossal* type) results in the greatest expansion of the posterior roof module (red), suggesting high biting forces by joined action of AMEP, AMES, AMP, and AMEM. The otic notch in some potential stem-amniotes like Seymoriamorpha mirrors the modeled upper temporal excavation (Klembara, 1997, 2011). It is likely that these animals were already adapted to a more or less full terrestrial life style with a focus on hard terrestrial food items. Also, strong biting turtles such as Chelydridae, Pelomedusidae, and Platysternidae (Herrel et al., 2002; Ferreira et al., 2020) develop deep upper temporal excavations (posterodorsal emarginations in turtle anatomical terminology *sensu* Werneburg, 2012).

From Robust to Agile—and Back to Robust Prey: Diapsid Evolution

The presence of two temporal openings (*bifenestral-1* and *-2*) as seen in some early diapsids (**Figure 3G**: †*Petrolacosaurus*, **Figure 3H**: †*Youngina*) shows a cheek integration (orange) comparable to that of early synapsids (**Figure 3B**) with AMEP, AMES, AMP, and AMEM acting in union. This could highlight the generally stronger bite and, hence, better adaptation to terrestrial food in both diapsids and synapsids when compared to non-fenestrated early amniotes like †*C. aguti*.

Early diapsids are thought to have been adapted to feeding on agile prey (Evans, 2008), for which an increased intracranial mobility was necessary (see discussion further below). More crownward diapsids (Lee et al., 2020; Plateau and Foth, 2020) differ from the modeled early diapsids. Differences are likely associated with a change to a more carnivorous feeding behavior as exemplified in archosauriform evolution with †*Euparkeria capensis* representing a transitional form (Sookias et al., 2020) or †*Tyrannosaurus rex* showing specific snout adaptations (Werneburg et al., 2019). The relatively larger snouts, together with the orbits, increasingly restricted the space for the temporal region through archosaur evolution. Related to strong bites and long snouts, the pterygoid musculature in crocodiles dominates above the external jaw adductors with influence on bone arrangements and modularity in the respective regions as illustrated by *Alligator mississippiensis* (Werneburg et al., 2019).

The textbook example of an extant diapsid, the tuatara *Sphenodon punctatus* (Lepidosauria), is also highly derived in its skull network modularity (Werneburg et al., 2019) when compared to the herein modeled early diapsid forms. Tuatara secondarily re-evolved the lower temporal arcade (Müller, 2003) and has a number of other derived characters. The degree of its intracranial mobility is debated and seems to depend on ontogenetic changes with, likely, less mobile skulls and stronger bites in adults (Jones et al., 2011; Werneburg and Yaryhin, 2019).

The Never-Ending Turtle Story

The *bifossal* model (**Figure 3I**) resembles a morphotype that is basically established in the turtle crown-group (Werneburg, 2012), a group that reportedly shows several derived characters compared to the ancestral amniote and even to the ancestral turtle condition (Müller, 2003; Joyce, 2007). Hence, the limitation mentioned above for interpreting a network model also applies, particularly, when discussing the turtle skull morphotype. Nevertheless, the simplification in the network methodology permits a comparison to other models.

Compared to †*C. aguti*, the jugal in the *bifossal* model becomes part of the snout flank module (light purple), mirrored by the general robusticity of the snout in turtles, which is ancestrally covered by an edentulous beak (Li et al., 2018). The remainder of the temporal region forms one consistent module (red) likely related to a union of AMEP, AMES, and AMP (**Figure 3I**). In fact, jaw musculature in turtles is (superficially) less diverse than that of all other extant reptilian groups (Schumacher, 1956; Werneburg, 2011, 2013a,b).

With the formation of a deep ventral excavation, the skull network, again, separates into an anterior and a posterior skull part. Whereas this feature resulted in a supposedly

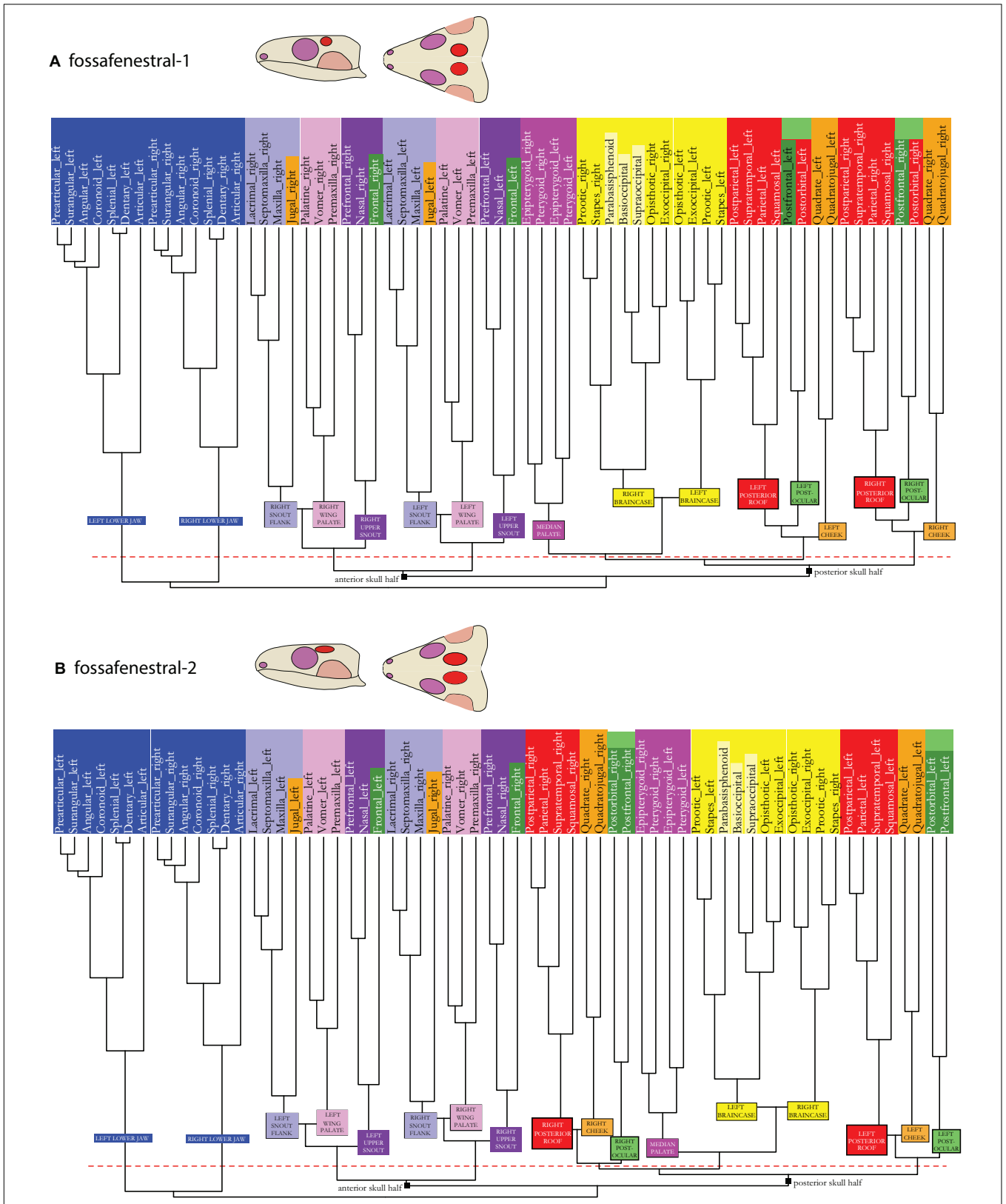

FIGURE 8 | (Continued)

FIGURE 8 | Dendrogram of the skull network of **(A)** the *fossafenestral-1* and **(B)** the *fossafenestral-2* skull types. Compare to caption of **Figure 2E**. The basal dichotomies in an anterior and a posterior skull part are indicated in the dendrogram.

higher independency and mobility of the epipterygoid (dark pink) in taxa like millerettids, †*Microleter*, and †*Eunotosaurus* (**Figure 3D**), the epipterygoid is either lost (Pleurodira) or integrated (Cryptodira) into the secondary braincase wall in crown-turtles (Werneburg and Maier, 2019), decoupling this element from other skull modules (which is associated with the loss of CID musculature in turtles; see Werneburg, 2011) and resulting in an akinetic skull (Werneburg and Maier, 2019). As has been shown by Ferreira et al. (2020), the jaw muscle arrangement and the skull shape of modern turtles is associated with fundamental cranial changes related to the evolutionary increase of neck mobility. Jaw muscle functionality can be seen as a tradeoff between restrictions in space for jaw musculature in the jaw adductor chamber and the retention (but not increase) of the ancestral jaw muscle power. While the jaw musculature of turtles is rather simple in superficial view, it internally shows great tendinous differentiation, which might reflect the concealed anatomical response to that restriction (Schumacher, 1956; Werneburg, 2011, 2013b).

The expansion of the posterior skull roof module (red) in the *bifossal* turtle skull can be associated with a higher integration related to neck mobility. Tensional force of the retracting neck is related to enlarged temporal emarginations (Werneburg, 2012, 2015) and might be buffered by a broadly integrated temporal region (Werneburg et al., 2021).

The leatherback turtle, *Dermochelys coriacea* (Werneburg et al., 2019), largely reduced its ability to retract the neck and, hence, no posterodorsal emarginations are developed in the skull (*sensu* Werneburg, 2015). Notably, in the anatomical network reconstructed for this species, only an integration of frontal and parietal, but not of the cheek region, is present. The close association of frontal and parietal can be interpreted by a still certain degree of embryonic neck muscle tension acting on the roof of its developing skull (Werneburg and Maier, 2019; Werneburg et al., 2021). Different to our model (**Figure 3I**), an ancestral integration of the jugal into the cheek module (orange) is present in the leatherback. This can be interpreted by the specific arrangement of bones, related to unique characters such as a truncated snout and a domed skull in this marine turtle species (Nick, 1912; Schumacher, 1972; Werneburg et al., 2019).

Notably, the *bifossal* skull type (**Figure 3I**) is also present in the akinetic mammals, although the upper temporal excavation derives from an expanded upper temporal fenestra and not by marginal bone reductions (Werneburg, 2019). The convergent separation in an anterior and a posterior skull part and a related simplification of skull network composition (Werneburg et al., 2019) is stunning.

Toward Highly Kinetic Skulls

Whether a *fossafenestral-1* type (**Figure 3J**) was actually developed in †*Claudiosaurus* is debatable based on whether and how much the postfrontal actually contributed to the upper temporal opening (Carroll, 1981). Nevertheless, when compared to the *fossafenestral-2* type (**Figure 3K**), in which the upper temporal opening expands more anteriorly, the general size-influence of an opening becomes obvious, as in this example the posterior skull roof module (red) changes its global modular association (see dendrogram in **Figure 8B** and white parallel stripes in **Figure 3K**).

Among early amniotes, the *fossafenestral-2* type is likely present in †tangasaurids (Bickelmann et al., 2009) and basically represents the skull type found among the neodiapsid squamates. Whenever an upper temporal fenestra is formed together with a lower temporal excavation (**Figures 3C,J–K**), a postocular module (light green) emerges. The same is true for the *bifenestral* skull, in which the supratemporal fenestra is anteriorly expanded (*bifenestral-2* type; **Figure 3H**) as is known for †*Youngina* among early amniotes. Different muscle portions that mainly attach to other bones (star in **Figure 3A**) can partly originate or insert also to the postorbital in extant reptiles (Holliday and Witmer, 2007; Werneburg, 2013a). Having a postocular skull module (light green), which includes postorbital and postfrontal, could indicate to more independent differentiation of those muscle fibers attaching there. Consequently, number and effective direction of muscle vectors will change. As virtually all external adductor muscles insert to the lower jaw, a more complex positioning of agile prey in the mouth can be assumed, as reflected by the insectivorous diet of many taxa with *fossafenestral-2* skull anatomy (i.e., squamates), but also in taxa with *infrafenestral-2* skulls, such as therapsids, which are "on their way" to develop chewing behavior with increased jaw mobility.

The infratemporal openings of *fossafenestral* forms, again, split the skull in an anterior and a posterior part. The epipterygoid (dark pink), with its reconstructed independent CID musculature, could, again, serve as pivot point, in these taxa and enable amphikinetic skull movements (Iordansky, 1990, 2011). In all models described, and in †*C. aguti*, the epipterygoids and pterygoids with their associated musculature form a single module (dark pink), suggesting that they might act together. Whereas the epipterygoid is originally used as lever arm to move the palate in anteroposterior direction—which might still be the case in most taxa—it appears to further act in positioning the pterygoid when handling diverse food items in *bifenestral-2* and *fossafenestral* skulls. In this regard, the former, represented by †*Youngina*, represents a transitional state toward the highly kinetic skull of squamate reptiles.

CONCLUSIONS

Our study tackles one of the big questions in vertebrate evolutionary morphology, namely, the evolution and functional meaning of temporal skull openings in amniotes. Although the used anatomical network theory has a number of limitations due to its simplifying methodology, it allows strategical comparisons among different anatomical models. A careful evaluation of the

observed outcome is necessary and requires a comprehensive morphological discussion.

Here, we modeled the presence or absence of temporal openings into a given skull network to observe the effect on module composition. We demonstrated that changes in the number, position, and expansion of temporal openings have fundamental impact on skull modularity. This is interpreted mainly in regard to feeding behavior in amniotes, where the assumed hardness and agility of prey items are considered. Changes in temporal openings and the resulting skull modules also have impact on cranial kinesis.

The present discussion is highly speculative and remains at a modeling level. It should be understood as a first attempt to interpret complex skull modularity in early amniotes. Obviously, actual skulls need to be studied and coded to get a clearer picture of network modularity in early amniote skulls. By presenting the skull network modularity of the well-known †*C. aguti*, we provide a first attempt in this direction.

A comparison with crown-group amniote skulls, finally, supports the basic functional assumptions that we have derived from our modeling approach. Influenced by changed feeding adaptations and associated changes in skull architecture, however, secondary alterations from the ancestral amniote skull network conditions evolved in crownward taxa. Detecting and describing general patterns of changes across amniote evolution is a desirable outlook on future broad scale taxonomic analysis using the anatomical network methodology.

DATA AVAILABILITY STATEMENT

The original contributions presented in the study are included in the article/**Supplementary Material**, further inquiries can be directed to the corresponding author.

AUTHOR CONTRIBUTIONS

IW: conceptualization, data interpretation, figure preparation, and writing. PA: data acquisition, analysis, and careful annotations on the manuscript. Both authors contributed to the article and approved the submitted version.

ACKNOWLEDGMENTS

We wish to thank Borja Esteve-Altava (Heidelberg), Gerardo Antonio Cordero (Lisbon), and Oleksandr Yaryhin (Plön) for discussion on AnNA-methodology. Diego Rasskin-Gutman and Eduardo Ascarrunz are thanked for critical reading and suggestions to improve the article. This study was supported by DFG-fund WE 5440/6-1 granted to IW.

SUPPLEMENTARY MATERIAL

The Supplementary Material for this article can be found online at: https://www.frontiersin.org/articles/10.3389/fevo.2021.799637/full#supplementary-material

REFERENCES

Abdala, F., and Damiani, R. (2004). Early development of the mammalian superficial masseter muscle in cynodonts. *Palaeontol. Afr.* 40, 23–29.

Abel, P., Pommery, Y., Ford, D. P., Koyabu, D., and Werneburg, I. (2022). "Skull sutures and cranial mechanics in the Permian reptile *Captorhinus aguti* and the evolution of the temporal region in early amniotes," In *The Temporal Region of the Tetrapod Skull Research History, Evolution, and Functional Backgrounds. Dissertation* (Tübingen: University of Tübingen).

Abel, P., and Werneburg, I. (2021). Morphology of the temporal skull region in tetrapods: research history, functional explanations, and a new comprehensive classification scheme. *Biol. Rev.* 96, 2229–2257. doi: 10.1111/brv.12751

Berman, D. S., and Reisz, R. R. (1986). Captorhinid reptiles from the Early Permian of New Mexico, with description of a new genus and species. *Carnegie Mus. Nat. Hist.* 55, 1–28.

Bickelmann, C., Müller, J., and Reisz, R. R. (2009). The enigmatic diapsid *Acerosodontosaurus piveteaui* (Reptilia: Neodiapsida) from the Upper Permian of Madagascar and the paraphyly of "younginiform" reptiles. *Can. J. Earth Sci.* 46, 651–661. doi: 10.1139/E09-038

Bolt, J. R. (1974). Evolution and functional interpretation of some suture patterns in Paleozoic labyrinthodont amphibians and other lower tetrapods. *J. Paleontol.* 48, 434–458.

Bolt, J. R., and Rieppel, O. (2009). The holotype skull of *Llistrofus pricei* Carroll and Gaskill, 1978 (Microsauria: Hapsidopareiontidae). *J. Paleontol.* 83, 471–483. doi: 10.1666/08-076.1

Boonstra, L. D. (1952). N nuwe soort van tapinocephalide deinocephaliër *Struthiocephalus akraalensis* sp. nov. *South Afr. J. Sci.* 48, 247–248.

Bramble, D., and Wake, D. (1985). *Feeding Mechanisms of Lower Tetrapods. In: Functional Vertebrate Morphology*. Cambridge: Harvard University Press, 230–261. doi: 10.4159/harvard.9780674184404.c13

Broom, R. (1922). On the Temporal Arches of the Reptilia. *Proc. Zool. Soc. Lond.* 92, 17–26. doi: 10.1111/j.1096-3642.1922.tb03297.x

Burne, R. H. (1905). Notes on the muscular and visceral anatomy of leathery turtle (*Dermochelys coriacea*). *Proc. Zool. Soc. Lond.* 75, 291–324. doi: 10.1111/j.1469-7998.1905.tb00001.x

Carroll, R. L. (1969). Problems of the origins of reptiles. *Biol. Rev.* 44, 393–432. doi: 10.1111/j.1469-185X.1969.tb01218.x

Carroll, R. L. (1981). Plesiosaur ancestors from the Upper Permian of Madagascar. *Philos. Trans. R. Soc. Lond. Ser. B Biol. Sci.* 293, 315–383. doi: 10.1098/rstb.1981.0079

Case, E. C. (1898). The significance of certain changes in the temporal region of the primitive Reptilia. *Am. Nat.* 32, 69–74. doi: 10.1086/276778

Case, E. C. (1911). *A Revision of the Cotylosauria of North America*. Washington: Carnegie Institution of Washington. doi: 10.5962/bhl.title.45604

Case, E. C. (1924). A possible explanation of fenestration in the primitive reptilian skull, with notes on temporal region of the genus *Dimetrodon*. *Contrib. Mus. Geol. Univ. Mich.* 2, 1–12.

Cisneros, J. C., Damiani, R., Schultz, C., da Rosa, Á, Schwanke, C., Neto, L. W., et al. (2004). A procolophonoid reptile with temporal fenestration from the Middle Triassic of Brazil. *Proc. R. Soc. Lond. B* 271, 1541–1546. doi: 10.1098/rspb.2004.2748

Clack, J., and Carroll, R. L. (1973). Romeriid reptiles from the Lower Permian. *Bull. Mus. Comp. Zool.* 144, 353–407.

Clack, J. A. (2012). *Gaining Ground. The Origin and Evolution of Tetrapods. Second Edition*. Bloomington: Indiana University Press.

Csardi, G., and Nepusz, T. (2006). The igraph software package for complex network research. *Int. J. Complex Syst.* 1659, 1–9.

Currie, P. J. (1981). *Hovasaurus boulei*, an aquatic eosuchian from the Upper Permian of Madagascar. *Palaeontol. Afr.* 24, 99–168.

Diogo, R., and Abdala, V. (2010). *Muscles of Vertebrates*. Enfield: Science Publishers. doi: 10.1201/9781439845622

Diogo, R., Esteve-Altava, B., Smith, C., Boughner, J. C., and Rasskin-Gutman, D. (2015). Anatomical network comparison of human upper and lower, newborn and adult, and normal and abnormal limbs, with notes on development, pathology and limb serial homology vs. homoplasy. *PLoS One* 10:e0140030. doi: 10.1371/journal.pone.0140030

Dodick, J. T., and Modesto, S. P. (1995). The cranial anatomy of the captorhinid reptile *Labidosaurikos meachami* from the Lower Permian of Oklahoma. *Palaeontology* 38, 687–711.

Elzanowski, A., and Mayr, G. (2018). Multiple origins of secondary temporal fenestrae and orbitozygomatic junctions in birds. *J. Zool. Syst. Evol. Res.* 56, 248–269. doi: 10.1111/jzs.12196

Esteve-Altava, B. (2017a). Challenges in identifying and interpreting organizational modules in morphology. *J. Morphol.* 278, 960–974. doi: 10.1002/jmor.20690

Esteve-Altava, B. (2017b). In search of morphological modules: a systematic review. *Biol. Rev.* 92, 1332–1347. doi: 10.1111/brv.12284

Esteve-Altava, B. (2017c). Network Models: connecting Anatomy to Systems Biology. *FASEB J.* 386.2.

Esteve-Altava, B., Boughner, J., Diogo, R., and Rasskin-Gutman, D. (2015a). Anatomical network analysis of primate skull morphology. *FASEB J.* 29:867.3. doi: 10.1096/fasebj.29.1_supplement.867.3

Esteve-Altava, B., Boughner, J. C., Diogo, R., Villmoare, B. A., and Rasskin-Gutman, D. (2015b). Anatomical network analysis shows decoupling of Modular lability and complexity in the evolution of the primate skull. *PLoS One* 10:e0127653. doi: 10.1371/journal.pone.0127653

Esteve-Altava, B., Diogo, R., Smith, C., Diego, J. C. B., and Rasskin-Gutman, D. (2015c). Anatomical networks reveal the musculoskeletal modularity of the human head. *Sci. Rep.* 5:8298. doi: 10.1038/srep08298

Esteve-Altava, B., Marugan-Lobon, J., Botella, H., Bastir, M., and Rasskin-Gutman, D. (2013a). Grist for Riedl's Mill: a network model perspective on the integration and modularity of the human skull. *J. Exp. Zool. B Mol. Dev. Evol.* 320, 489–500. doi: 10.1002/jez.b.22524

Esteve-Altava, B., Marugan-Lobon, J., Botella, H., and Rasskin-Gutman, D. (2013b). Structural constraints in the evolution of the tetrapod skull complexity: Williston's Law revisited using network models. *Evol. Biol.* 40, 209–219. doi: 10.1007/s11692-012-9200-9

Esteve-Altava, B., Marugan-Lobon, J., Botella, H., and Rasskin-Gutman, D. (2011). Network Models in Anatomical Systems. *J. Anthropol. Sci.* 89, 175–184.

Evans, S. E. (2008). "The Skull of Lizards and Tuatara," in *Morphology H: The Skull of the Lepidosauria*, eds C. Gans, A. S. Gaunt, and K. Adler (Salt Lake City: Society for the Study of Amphibians and Reptiles), 1–347.

Ferreira, G. S., Lautenschlager, S., Evers, S. W., Pfaff, C., Kriwet, J., Raselli, I., et al. (2020). Feeding biomechanics suggests progressive correlation of skull architecture and neck evolution in turtles. *Sci. Rep.* 10:5505. doi: 10.1038/s41598-020-62179-5

Ford, D. P. (2018). *The Evolution and Phylogeny of Early Amniotes*. Ph.D. thesis. Oxford: University of Oxford.

Fox, R. C. (1964). The adductor muscles of the jaw in some primitive reptiles. *Univ.Kans. Publ. Mus. Nat. His.* 12, 657–680.

Fox, R. C., and Bowman, M. C. (1966). Osteology and relationships of *Captorhinus aguti* (Cope) (Reptilia: Captorhinomorpha). *Univ. Kans. Paleontol. Contrib.* 11, 1–79.

Frazzetta, T. (1968). Adaptive problems and possibilities in the temporal fenestration of tetrapod skulls. *J. Morphol.* 125, 145–157. doi: 10.1002/jmor.1051250203

Frey, E., Tarsitano, S., Oelofsen, B., and Riess, J. (2001). The origin of temporal fenestrae. *South Afr. J. Sci.* 97, 334–336.

Gaffney, E. S. (1979). Comparative cranial morphology of recent and fossil turtles. *Bull. Am. Mus. Nat. Hist.* 164, 67–376.

Gaffney, E. S. (1990). The comparative osteology of the Triassic turtle *Proganochelys*. *Bull. Am. Mus. Nat. Hist.* 194:263.

Gow, C. (1972). The osteology and relationships of the Millerettidae (Reptilia: Cotylosauria). *J. Zool.* 167, 219–264. doi: 10.1111/j.1469-7998.1972.tb01731.x

Gow, C. E. (1997). A reassessment of *Eunotosaurus africanus* Seeley (Amniota: Parareptilia). *Palaeontol. Afr.* 34, 33–42.

Hall, B. K. (2005). *Bones and Cartilage: Developmental and Evolutionary Skeletal Biology*. Cambridge: Elsevier Academic Press. doi: 10.1016/B978-0-12-319060-4.50065-8

Hall, B. K. (2009). *The Neural Crest and Neural Crest Cells in Vertebrate Development and Evolution*. New York: Springer. doi: 10.1007/978-0-387-09846-3

Hanken, J., and Hall, B. (eds) (1993a). *The Skull. Vol 2, Patterns of Structural and Systematic Diversity*. Chicago: The University of Chicago Press.

Hanken, J., and Hall, B. (eds) (1993b). *The Skull. Vol 3, Functional and Evolutionary Mechanisms*. Chicago: The University of Chicago Press.

Haridy, Y., Macdougall, M. J., Scott, D., and Reisz, R. R. (2016). Ontogenetic change in the temporal region of the early Permian parareptile *Delorhynchus cifellii* and the implications for closure of the temporal fenestra in amniotes. *PLoS One* 11:e0166819. doi: 10.1371/journal.pone.0166819

Heiss, E., Natchev, N., Gumpenberger, M., Weissenbacher, A., and Van Wassenbergh, S. (2013). Biomechanics and hydrodynamics of prey capture in the Chinese giant salamander reveal a high-performance jaw-powered suction feeding mechanism. *J. R. Soc. Interface* 10:20121028. doi: 10.1098/rsif.2012.1028

Herrel, A., O'Reilly, J. C., and Richmond, A. M. (2002). Evolution of bite performance in turtles. *J. Evolu. Biol.* 15, 1083–1094. doi: 10.1046/j.1420-9101.2002.00459.x

Higashiyama, H., Koyabu, D., Hirasawa, T., Werneburg, I., Kuratani, S., and Kurihara, H. (2021). Mammalian face as an evolutionary novelty. *Proc. Nat. Acad. Sci. U. S, A.* 118:e2111876118. doi: 10.1073/pnas.2111876118

Holliday, C. M., and Witmer, L. M. (2007). Archosaur adductor chamber evolution: Integration of musculoskeletal and topological criteria in jaw muscle homology. *J. Morphol.* 268, 457–484. doi: 10.1002/jmor.10524

Holmes, R. (1984). The Carboniferous amphibian *Proterogyrinus scheelei* Romer, and the early evolution of tetrapods. *Philos. Trans. R. Soc. Lond. B Biol. Sci.* 306, 431–524. doi: 10.1098/rstb.1984.0103

Hülsmann, E., and Wahlert, G. V. (1972). *Das Schädelkabinett - Eine erklärende Naturgeschichte der Wirbeltiere*. Basel: Basilius Presse.

Iordansky, N. (1990). Evolution of cranial kinesis in lower tetrapods. *Neth. J. Zool.* 40, 32–54. doi: 10.1163/156854289X00174

Iordansky, N. N. (2011). Cranial kinesis in lizards (*Lacertilia*): origin, biomechanics, and evolution. *Biol. Bull.* 38, 852–861. doi: 10.1134/S1062359011090032

Jaeckel, O. (1902). Ueber *Gephyrostegus bohemicus*. *Zeitschrift der Deutschen Geologischen Gesellschaft* 54, 127–133.

Jones, M. E. H., Curtis, N., Fagan, M. J., O'Higgins, P., and Evans, S. E. (2011). Hard tissue anatomy of the cranial joints in *Sphenodon* (Rhynchocephalia): sutures, kinesis, and skull mechanics. *Palaeontol. Electron.* 14:33604.

Jones, M. E. H., Curtis, N., O'Higgins, P., Fagan, M., and Evans, S. E. (2009). The head and neck muscles accociated with feeding on *Sphenodon* (Reptilia: Lepidosauria: Rynchocephalia). *Palaeontol. Electron.* 12:56.

Joyce, W. G. (2007). Phylogenetic relationships of Mesozoic turtles. *Bull. Peabody Mus. Nat. Hist.* 48, 3–102. doi: 10.3374/0079-032X(2007)48[3:PROMT]2.0.CO;2

Kammerer, C. F. (2011). Systematics of the Anteosauria (Therapsida: Dinocephalia). *J. Syst. Palaeontol.* 9, 261–304. doi: 10.1080/14772019.2010.492645

Kemp, T. S. (1980). Origin of the mammal-like reptiles. *Nature* 283, 378–380. doi: 10.1038/283378a0

Kemp, T. S. (1982). *Mammal-Like Reptiles and the Origin of Mammals*. Cambridge: Academic Press.

Keyser, A. W., and Gow, C. E. (1981). First complete skull of the Permian reptile *Eunotosaurus africanus* Seeley. *South Afr. J. Sci.* 77, 417–421.

Klembara, J. (1997). The cranial anatomy of *Discosauriscus* Kuhn, a seymouriamorph tetrapod from the Lower Permian of the Boskovice Furrow (Czech Republic). *Philos. Trans. R. Soc. Lond. B.* 352, 257–302. doi: 10.1098/rstb.1997.0021

Klembara, J. (2011). The cranial anatomy, ontogeny, and relationships of *Karpinskiosaurus secundus* (Amalitzky) (Seymouriamorpha, Karpinskiosauridae) from the Upper Permian of European Russia. *Zool. J. Linn. Soc.* 161, 184–212. doi: 10.1111/j.1096-3642.2009.00629.x

Klembara, J., Berman, D. S., Henrici, A. C., Cernansky, A., and Werneburg, R. (2006). Comparison of cranial anatomy and proportions of similarly sized *Seymouria sanjuanensis* and *Discosauriscus austriacus*. *Ann. Carnegie Mus.* 30, 37–49. doi: 10.2992/0097-4463(2006)75[37:COCAAP]2.0.CO;2

Klembara, J., Tomasik, A., and Kathe, W. (2002). Subdivisions, fusions and extended sutural areas of dermal skull bones in *Discosauriscus* KUHN (Seymouriamorpha). *Neues Jahrbuch für Geologie und Paläontologie Abhandlungen* 223, 317–349. doi: 10.1127/njgpa/223/2002/317

Koyabu, D., Werneburg, I., Morimoto, N., Zollikofer, C. P. E., Forasiepi, A. M., Endo, H., et al. (2014). Mammalian skull heterochrony reveals modular evolution and a link between cranial development and brain size. *Nat. Commun.* 5:3625. doi: 10.1038/ncomms4625

Kuhn-Schnyder, E. (1980). "Observations on Temporal Openings of Reptilian Skulls and the Classification of Reptiles," in *Aspects of Vertebrate History, Essays in Honor of Edwin Harris Colbert*, ed. L. L. Jacobs (Flagstaff: Museum of Northern Arizona), 153–175.

Lakjer, T. (1926). *Studien über die Trigeminus-versorgte Kaumuskulatur der Sauropsiden*. Copenhagen: Reitsel Buchhandlung.

Lakjer, T. (1927). Studien über die Gaumenregion bei Sauriern im Vergleich mit Anamniern und primitiven Sauropsiden. *Zool. Jahrb.* 49, 57–356.

Laurin, M. (2005). Embryo retention, character optimization, and the origin of the extra-embryonic membranes of the amniotic egg. *J. Nat. Hist.* 39, 3151–3161. doi: 10.1080/00222930500300884

Laurin, M. (2010). *How Vertebrates Left the Water*. Los Angeles: University of California Press. doi: 10.1525/9780520947986

Lautenschlager, S., Gill, P., Luo, Z.-X., Fagan, M. J., and Rayfield, E. J. (2017). Morphological evolution of the mammalian jaw adductor complex: mammalian jaw muscle evolution. *Biol. Rev.* 92, 1910–1940. doi: 10.1111/brv.12314

LeBlanc, A. R. H., MacDougall, M. J., Haridy, Y., Scott, D., and Reisz, R. R. (2018). Caudal autotomy as anti-predatory behaviour in Palaeozoic reptiles. *Sci. Rep.* 8:3328. doi: 10.1038/s41598-018-21526-3

Lee, H. W., Esteve-Altava, B., and Abzhanov, A. (2020). Evolutionary and ontogenetic changes of the anatomical organization and modularity in the skull of archosaurs. *Sci. Re.* 10:16138. doi: 10.1038/s41598-020-73083-3

Li, C., Fraser, N. C., Rieppel, O., and Wu, X. C. (2018). A Triassic stem turtle with an edentulous beak. *Nature* 560, 476–479. doi: 10.1038/s41586-018-0419-1

Lucas, S. G., Rinehart, L. F., and Celeskey, M. D. (2018). The oldest specialized tetrapod herbivore: a new eupelycosaur from the Permian of New Mexico, USA. *Palaeontol. Electron.* 21, 1–42. doi: 10.26879/899

MacDougall, M. J., and Reisz, R. R. (2014). The first record of a nyctiphruretid parareptile from the early Permian of North America, with a discussion of parareptilian temporal fenestration. *Zool. J. Linn. Soc.* 172, 616–630. doi: 10.1111/zoj.12180

Maier, W. (1989). "Ala Temporalis and Alisphenoid in Therian Mammals," in *Trends in Vertebrate Morphology*, eds H. Splechtna and H. Hilgers (Stuttgart: Fischer Verlag), 396–400.

Maier, W. (1999). On the evolutionary biology of early mammals - with methodological remarks on the interaction between ontogenetic adaptation and phylogenetic transformation. *Zool. Anz.* 238, 55–74.

Maier, W., and Werneburg, I. (2014). *Einführung: Zur Methodik der organismischen Evolutionsbiologie. In: Maier W, Werneburg I. Schlüsselereignisse der organismischen Makroevolution*. Zürich: Scidinge Hall Verlag, 11–17.

Mann, A., Pardo, J. D., and Maddin, H. C. (2019). *Infernovenator steenae*, a new serpentine recumbirostran from the 'Mazon Creek' Lagerstätte further clarifies lysorophian origins. *Zool. J. Linn. Soc.* 187, 506–517. doi: 10.1093/zoolinnean/zlz026

Modesto, S. P. (1995). The skull of the herbivorous synapsid *Edaphosaurus boanerges* from the Lower Permian of Texas. *Palaeontology* 38, 213–239.

Modesto, S. P. (1998). New information on the skull of the Early Permian reptile *Captorhinus aguti*. *Paleobios* 18, 21–35.

Molnar, J., Esteve-Altava, B., Rolian, C., and Diogo, R. (2017). Comparison of musculoskeletal networks of the primate forelimb. *Sci. Rep.* 7:10520. doi: 10.1038/s41598-017-09566-7

Müller, J. (2003). Early loss and multiple return of the lower temporal arcade in diapsid reptiles. *Naturwissenschaften* 90, 473–476. doi: 10.1007/s00114-003-0461-0

Müller, J., and Reisz, R. R. (2005). An early captorhinid reptile (Amniota, Eureptilia) from the Upper Carboniferous of Hamilton, Kansas. *J. Vertebr. Paleontol.* 25, 561–568. doi: 10.1671/0272-4634(2005)025[0561:AECRAE]2.0.CO;2

Natchev, N., Handschuh, S., Lukanov, S., Tzankov, N., Naumov, B., and Werneburg, I. (2016). Contributions to the functional morphology of caudate skulls: kinetic and akinetic forms. *PeerJ* 4:e2392. doi: 10.7717/peerj.2392

Natchev, N., Tzankov, N., Werneburg, I., and Heiss, E. (2015). Feeding behaviour in a 'basal' tortoise provides insights on the transitional feeding mode at the dawn of modern land turtle evolution. *PeerJ* 3:e1172. doi: 10.7717/peerj.1172

Nick, L. (1912). Das Kopfskelett von *Dermochelys coriacea* L. *Zoologische Jahrbücher, Abteilung für Anatomie und Ontogenie der Tiere* 33, 1–238.

Novacek, M. J. (1993). "Patterns of Diversity in the Mammalian Skull," in *The Skull, Volume 2: Patterns of Structural and Systematic Diversity*, eds J. Hanken and B. Hall (Chicago: University of Chicago Press), 438–545.

Panchen, A. L. (1964). The cranial anatomy of two coal measure anthracosaurs. *Philos. Trans. R. Soc.* 247, 593–637. doi: 10.1098/rstb.1964.0006

Plateau, O., and Foth, C. (2020). Birds have peramorphic skulls, too: anatomical network analyses reveal oppositional heterochronies in avian skull evolution. *Commun. Biol.* 3:195. doi: 10.1038/s42003-020-0914-4

Polachowski, K. M., and Werneburg, I. (2013). Late embryos and bony skull development in *Bothropoides jararaca* (Serpentes, Viperidae). *Zoology* 116, 36–63. doi: 10.1016/j.zool.2012.07.003

R Core Team (2020). *R: A language and environment for statistical computing*. Vienna: R Foundation for Statistical Computing. URL. https://www.R-project.org/

Rasskin-Gutman, D. (2003). "Boundary Constraints for the Emergence of Form," in *Origination of Organismal Form. Beyond the Gene in Developmental and EvolutionaryBiology*, eds G. B. Müller and S. A. Newman (Cambridge: MIT Press), 305–322.

Rasskin-Gutman, D., and Esteve-Altava, B. (2014). Connecting the dots: anatomical network analysis in morphological EvoDevo. *Biol. Theory* 9, 178–193. doi: 10.1007/s13752-014-0175-x

Rasskin-Gutman, D., and Esteve-Altava, B. (2021). "Concept of Burden in Evo-Devo," in *Evolutionary Developmental Biology. A Reference Guide*, eds L. Nuño de la Rosa and G. B. Müller (Berlin: Springer), 39–49. doi: 10.1007/978-3-319-32979-6_48

Reisz, R. R. (1977). *Petrolacosaurus*, the oldest known diapsid reptile. *Science* 196, 1091–1093. doi: 10.1126/science.196.4294.1091

Reisz, R. R., Berman, D. S., and Scott, D. (1984). The anatomy and relationships of the Lower Permian reptile *Araeoscelis*. *J. Vertebr. Paleontol.* 4, 57–67. doi: 10.1080/02724634.1984.10011986

Reisz, R. R., Schoch, R. R., and Anderson, J. S. (2009). The armoured dissorophid *Cacops* from the Early Permian of Oklahoma and the exploitation of the terrestrial realm by amphibians. *Naturwissenschaften* 96, 789–796. doi: 10.1007/s00114-009-0533-x

Rieppel, O. (1984). The upper temporal arcade of lizards: an ontogenetic problem. *Revue suisse Zool.* 91, 475–482. doi: 10.5962/bhl.part.81891

Rieppel, O. (1987). The development of the trigeminal jaw adductor musculature and associated skull elements in the lizard *Podarcis sicula*. *J. Zool.* 212, 131–150. doi: 10.1111/j.1469-7998.1987.tb05120.x

Rieppel, O. (1993). "Patterns of Diversity in the Reptilian Skull," in *The Skull, Volume 2: Patterns of Structural and Systematic Diversity*, eds J. Hanken and B. Hall (Chicago: University of Chicago Press), 344–389.

Rieppel, O., and Gronowski, R. W. (1981). The loss of the lower temporal arcade in diapsid reptiles. *Zool. J. Linn. Soc.* 72, 203–217. doi: 10.1111/j.1096-3642.1981.tb01570.x

Romer, A. S., and Price, L. W. (1940). *Review of the Pelycosauria*. New York: Geological Society of America. doi: 10.1130/SPE28-p1

RStudio Team (2019). *RStudio: Integrated Development for R*. Boston, MA: RStudio, PBC.

Schumacher, G. H. (1956). Über die Fascien des Kopfes der Schildkröten nebst einigen Bemerkungen zu der Arbeit von Lakjer, 1926. *Zool. Anz.* 156, 35–54.

Schumacher, G. H. (1972). *Die Kopf- und Halsregion der Lederschildkröte* Dermochelys coriacea *(LINNAEUS 1766) - Anatomische Untersuchungen im Vergleich zu anderen rezenten Schildkröten - Mit 7 Figuren im Text und 31 Tafeln*. Berlin: Akademie-Verlag.

Schumacher, G. H. (1973). "The Head Muscles and Hyolaryngeal Skeleton of Turtles and Crocodilians," in *Biology of the Reptilia*, eds G. Gans and T. S. Parsons (New York: Academic Press).

Smith, H. M., Chiszar, D., and Frey, M. J. (1983). The terminology of amniote temporal vacuities. *Trans. Kans. Acad. Sci.* 86, 48–54. doi: 10.2307/3628423

Smith-Paredes, D., Núñez-León, D., Soto-Acuna, S., O'Connor, J., Botelho, J. F., and Vargas, A. O. (2018). Dinosaur ossification centres in embryonic birds uncover developmental evolution of the skull. *Nat. Ecol. Evol.* 2, 1966–1973. doi: 10.1038/s41559-018-0713-1

Sookias, R. B., Dilkes, D., Sobral, G., Smith, R. M. H., Wolvaardt, F. P., Arcucci, A. B., et al. (2020). The craniomandibular anatomy of the early archosauriform *Euparkeria capensis* and the dawn of the archosaur skull. *R. Soc. Open Sci.* 7:200116. doi: 10.1098/rsos.200116

Starck, D. (1995). *5. Teil: Säugetiere. 5/1: Allgemeines, Ordo 1-9*. Gustav: Fischer Verlag Jena.

Sues, H.-D., and Reisz, R. R. (1998). Origins and early evolution of herbivory in tetrapods. *Tree* 13, 141–145. doi: 10.1016/S0169-5347(97)01257-3

Sumida, S. S., and Martin, K. L. M. (eds) (1997). *Amniote Origins: Completing the Transition to Land*. San Diego: Academic Press.

Sushkin, P. P. (1928). Contributions to the cranial morphology of *Captorhinus* Cope (Reptilia, Cotylosauria, Captorhinidae). *Palaeobiologica* 1, 263–280.

Tarsitano, S. F., Oelofsen, B., Frey, E., and Riess, J. (2001). The origin of temporal fenestra. *South Afr. J. Sci.* 97, 334–336.

Tsuji, L. A., Müller, J., and Reisz, R. R. (2010). *Microleter mckinzieorum* gen. et sp. nov. from the Lower Permian of Oklahoma: the basalmost parareptile from Laurasia. *J. Syst. Palaeontol.* 8, 245–255. doi: 10.1080/14772010903461099

Van Den Heuvel, W. F. (1992). Kinetics of the skull in the chicken (*Gallus gallus domesticus*). *Neth. J. Zool.* 42, 461–582. doi: 10.1163/156854292X00071

Warren, J. W. (1961). The basicranial articulation of the early Permian cotylosaur, *Captorhinus*. *J. Paleontol.* 35, 561–563.

Watson, D. M. S. (1914). *Eunotosaurus africanus* Seeley, and the ancestry of the Chelonia. *Proc. Zool. Soc. Lond.* 11, 1011–1020.

Weishampel, D. B. (1997). Herbivory and reptiles. *Lethaia Rev.* 29:224. doi: 10.1111/j.1502-3931.1996.tb01654.x

Werneburg, I. (2011). The cranial musculature in turtles. *Palaeontol. Electron.* 14:99.

Werneburg, I. (2012). Temporal bone arrangements in turtles: an overview. *J. Exp. Zool. B Mol. Dev. Evol.* 318, 235–249. doi: 10.1002/jez.b.22450

Werneburg, I. (2013a). Jaw musculature during the dawn of turtle evolution. *Org. Divers. Evol.* 13, 225–254. doi: 10.1007/s13127-012-0103-5

Werneburg, I. (2013b). The tendinous framework in the temporal skull region of turtles and considerations about its morphological implications in amniotes: a review. *Zool. Sci.* 31, 141–153. doi: 10.2108/zsj.30.141

Werneburg, I. (2015). Neck motion in turtles and its relation to the shape of the temporal skull region. *C. R. Palevol* 14, 527–548. doi: 10.1016/j.crpv.2015.01.007

Werneburg, I. (2019). Morphofunctional categories and ontogenetic origin of temporal skull openings in amniotes. *Front. Earth Sci.* 7:13. doi: 10.3389/feart.2019.00013

Werneburg, I., Esteve-Altava, B., Bruno, J., Torres Ladeira, M., and Diogo, R. (2019). Unique skull network complexity of *Tyrannosaurus rex* among land vertebrates. *Sci. Rep.* 9:1520. doi: 10.1038/s41598-018-37976-8

Werneburg, I., Evers, S. E., and Ferreira, G. (2021). On the "cartilaginous rider" in the endocasts of turtle brain cavities. *Vertebr. Zool.* 71, 403–418.

Werneburg, I., and Maier, W. (2019). Diverging development of akinetic skulls in cryptodire and pleurodire turtles: an ontogenetic and phylogenetic study. *Vertebr. Zool.* 69, 113–143.

Werneburg, I., Polachowski, K., and Hutchinson, M. (2015). Bony skull development in the Argus monitor (Squamata, Varanidae, *Varanus panoptes*) with comments on developmental timing and adult anatomy. *Zoology* 118, 225–280. doi: 10.1016/j.zool.2015.02.004

Werneburg, I., and Yaryhin, A. (2019). Character definition and tempus optimum in comparative chondrocranial research. *Acta Zool.* 100, 376–388. doi: 10.1111/azo.12260

Williston, S. (1904). The temporal arches of the Reptilia. *Biol. Bull.* 7, 175–192. doi: 10.2307/1535794

Witzmann, F., and Werneburg, I. (2017). The palatal interpterygoid vacuities of temnospondyls and the implications for the associated eye- and jaw musculature. *Anat. Rec.* 300, 1240–1269. doi: 10.1002/ar.23582

Zdansky, O. (1923). Über die Temporalregion des Schildkrötenschädels. *Bull. Geol. Inst. Univ. Upsala* 19, 89–114.

Ziermann, J. M., Diaz, R. E., and Diogo, R. (2019). *Heads, Jaws, and Muscles: Anatomical, Functional, and Developmental Diversity in Chordate Evolution*. Cham: Springer. doi: 10.1007/978-3-319-93560-7

Zusi, R. L. (1993). "Patterns of Diversity in the Avian Skull," in *The Skull, Volume 2: Patterns of Structural and Systematic Diversity*, eds J. Hanken and B. Hall (Chicago: University of Chicago Press), 391–437.

Conflict of Interest: The authors declare that the research was conducted in the absence of any commercial or financial relationships that could be construed as a potential conflict of interest.

Publisher's Note: All claims expressed in this article are solely those of the authors and do not necessarily represent those of their affiliated organizations, or those of the publisher, the editors and the reviewers. Any product that may be evaluated in this article, or claim that may be made by its manufacturer, is not guaranteed or endorsed by the publisher.